Biomimetic Nanopores with Yeast Nucleoporins

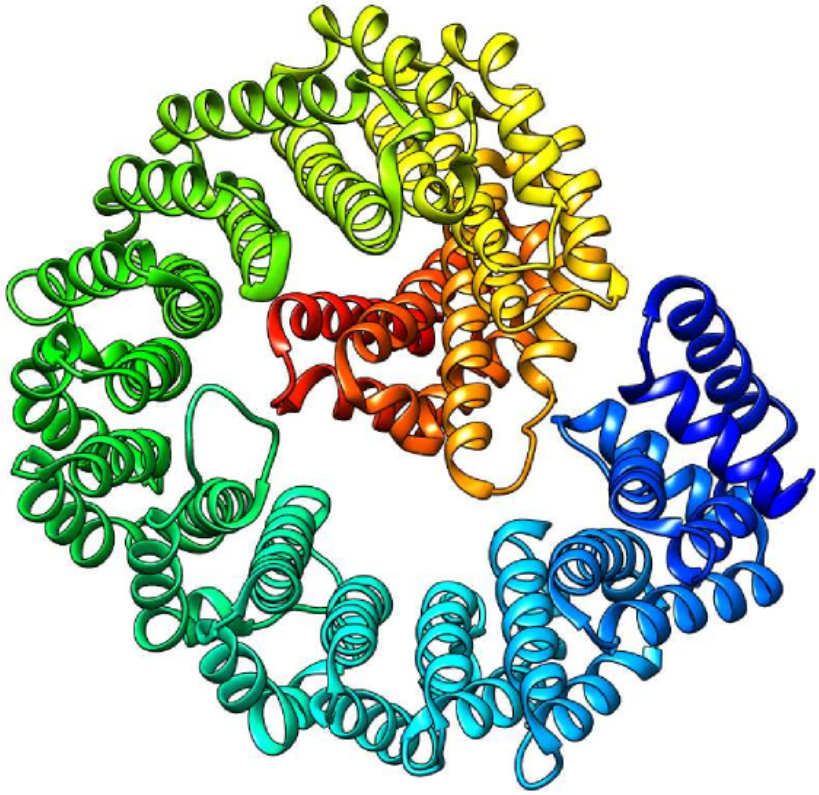

Arvind Dwarkasing

Bachelor Thesis

Supervisors: Adithya Ananth, Prof. Dr. Cees Dekker

August 27, 2014

Bionanoscience Department
Think big about life at the smallest scale

TU Delft Delft University of Technology
Challenge the future

Abstract

Nuclear pore complexes (NPC's) facilitate the exchange of macromolecules between the cytoplasm and nucleus and act as a selective barrier for macromolecules in eukaryotes. Ongoing research suggests that the discriminatory function of the NPC is caused by nucleoporins rich in phenylalanine-glycine amino acids residue repeats (FG-regions) which fill the nuclear pore. To determine if the FG-domains are responsible for the selectivity of a NPC, in this research we will mimic a nuclear pore complex by coating a solid state nanopore with yeast FG-nup-NSP1. After coating a wild-type nucleoporin, to a solid-state nanopore, we find that a yeast importer protein kap95 was able to translocate through the nanopore. The dwell times were on the order of tens of milliseconds. An artificial control protein, tCherry, with the same size as kap95, was not able to pass the artificial NPC. By coating a solid-state nanopore with mutated FG-nup-NSP1, where hydrophobic amino acid residues (F, I, L and V) were replaced with serine, we found that kap95 translocated with much lower translocation times, comparable to an uncoated nanopore, indicating less interaction with the mutated nucleoporins. Furthermore tCherry was also able to pass through the mimicked nuclear pore with mutated nucleoporins, making a very strong argument that FG-repeat regions in nucleoporins are responsible for the selectivity in NPC's.

Contents

1. Introduction

The nuclear pore complex plays a vital role in all eukaryotic cells as the only point where macromolecular exchange between nucleus and cytoplasm takes place. Because of the NPC's role as sole gatekeeper to the nucleus, research into its inner workings is great and over the last decades our understanding of their mechanisms has increased. The proteins making up the NPC, or for short nucleoporins, vary widely in size and composition.[1] It is now becoming clear that the nucleoporins rich in phenylalanine-glycine amino acid residues (FG-repeat regions) play a major role in the selective function of the NPC. For example, yeast cells in which the FG-repeats of the nucleoporins were replaced with other amino acids, could not be kept viable, indicating the disruption in transport into and out of the nucleus.[2]

Solid state nanopores have become a increasingly important tool over the past years to analyze proteins. A solid-state nanopore is a hole in an insulating membrane on the order of 1 - 100 nm. By translocating a protein through a nanopore, we are able to gain information on the proteins size, net charge and other characteristics.

If we combine a solid-state nanopore and nucleoporins, we are able to mimic a NPC at the simplest level. By attaching FG-rich nucleoporins to the solid-state nanopore, it has already been shown that the mimicked nanopore acts as a selective barrier.[3] In this research we will go one step further, which leads us to the objective of this research.

To prove that FG-nucleoporins are responsible for the selectivity in a NPC by creating biomimetic nuclear pores with wild-type and mutated nucleoporins

In this work we will build a biomimetic nanopore with a yeast nucleoporin, Nsp1 wild type. We will translocate two different types of protein through this artificial nanopore. The first protein is kap95, a transporter protein, which is able to pass through the NPC in yeast cells, so should also be able to translocate through our minimalistic replica of a nuclear pore. The second protein is tCherry, an artificial protein with the same size and weight as kap95. In theory, tCherry should not be able to translocate due to the selective feature of the FG-rich nucleoporins. The next step to complete the objective will be to create a second biomimetic nanopore, only this time with a mutated version of the Nsp1 wild type in which the hydrophobic amino acid residues have been replaced by serine, Nsp1 FILV $\rightarrow$ S. If the selectivity is lost, both proteins should pass through this nanopore or both proteins should fail to translocate.

In chapter 2 we will give a brief introduction on nuclear pore complexes, including the questions that are still unanswered about NPC's. In chapter 3 the theory behind solid-state nanopores will be treated and also how the measurements are carried out. Chapter 4 contains the methods to engineer the biomimetic nanopores. Chapter 5 contains the results of the measurements and a discussion on the outcomes. The last chapter, Chapter 6, will give a summary of the results and the conclusions we can make. In the final chapter there will also be a short outlook on future improvements.

2. Nuclear pore complex

An eukaryotic cell distinguishes itself from the prokaryotic counterpart by containing a nucleus. The nucleus contains the cells genetic material, which are DNA strings coiled up around nucleosomes to form chromosomes. This nucleus is separated from the rest of the cell by the nuclear envelope that comprises an inner and outer membrane. Transport of molecules from the cytoplasm to the nucleus and vice versa is an the most important process in a cell. For example, RNA carries genetic information from the DNA that is inside the nucleus, to ribosomes that are located outside the nucleus. This RNA gets translated in the cytoplasm and protein synthesis takes place. These proteins have critical functions inside every living organism. This nucleocytoplasmic transport is made possible by pores inside the double membrane that encloses the nucleus. These pores are called nuclear pore complexes (NPC's) and act as gatekeepers for transport to and from the nucleus. As early as 1950 the presence of these NPC was already determined by means of electron microscopy.[4] It was not until years later that their real importance became clear and technical advancements made it possible to study these NPC's in greater detail. They consist of a large number of proteins and are one of the largest protein structures inside a cell.[5] Every eukaryote has NPC's that cross its nuclear membrane and it is remarkable that even for different organisms the composition and morphology of the complex is conserved.[6]

In this project we'll be focusing on the NPC of Saccharomyces cerevisiae, a yeast species. It is a single celled fungi that has been extensively studied by scientist because it has a lot of favourable characteristics. A lot of the proteins in yeast have human homologs. Another advantage is that yeast can be genetically manipulated to tailor it to the needs of the research it is being used in. Saccharomyces cerevisiae is more commonly known as brewer's yeast to highlight its most important application, namely in the brewing process of wine and beer. As previously stated the NPC's of different organisms share a common architecture, so by studying the NPC of yeast we can get a better understanding of how nucleocytoplasmic transport in human cells work.

2.1 Architecture of NPC

The NPC is a highly sophisticated structure composed of a large number of different proteins. This means that if we want to get a complete picture of its morphology we have to use different techniques. For example, electron microscopy can be used to determine the symmetry of the NPC and then ultracentrifugation can be a tool to find out what proteins constitute the NPC. A lot more instruments can be deployed to get a good approximation of the true nature of a NPC. Based on the research by Alber et al.[7] we can get a good approximation on the physiology, inner workings and functions of a NPC.

The NPC of a yeast cell is composed of about 30 distinct proteins, which are named nucleoporins (short for nuclear pore proteins). The total number of nucleoporins making up the NPC is at least 456, meaning that it is a very large complex with a mass around the 50 MDa.[8] The NPC is highly symmetric and can be dissected into 8 spokes. As can

be seen from Figure 2.1 there are a lot of different sub-structures which themselves consist of a wide range of nucleoporins. The diameter of the channel is estimated to be around

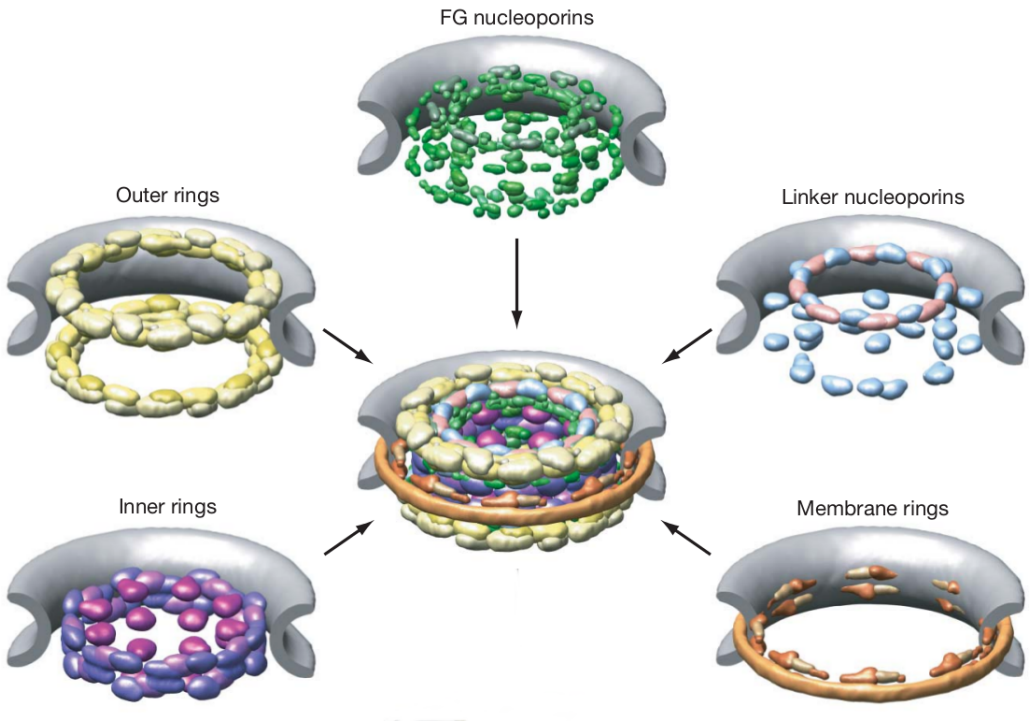

Figure 2.1: The architecture and composition of a yeast NPC.[9]

40nm, which also corresponds to the maximum size of known transported particles.[10] The diameter of the entire structure, including nucleoporins, is in the range of 100 nm and the height is around 40 nm. Most of the interactions between the nucleoporins are heterotypic, meaning that different protein types bind to each other. Every different substructure is believed to have a different function. For example, the membrane rings are responsible for anchoring the NPC to the nuclear envelope. There is still a lot of ongoing research to get a more complete picture of each component of the NPC. Especially the FG nucleoporins are under intense investigation because of their important role in the selective mechanism of the NPC, which will be further explained in section 1.3.

2.2 Transport through the NPC

Transport in and out of the nucleus is a vital function for life. It is estimated that in humans every minute more than one kilogram of material is shuttled across the NPC's in our body.[11] This highlights the efficiency and capabilities of the extremely complicated structure.

As mentioned earlier, there is a selective channel running through the central part of the NPC. In the past, research suggested that this central channel only accommodated active transport and that other particles passively diffused through smaller holes in the NPC, such as those between the outer rings and the nuclear envelope. Recently it was shown that also passive transport relies on the main channel of the NPC.[12] This passive

diffusion of molecules through the NPC is limited to smaller particles, up to about 40 kDa or if the molecule has a hydrodynamic radius smaller than 5nm. Macromolecules which are larger than the criteria face a selection mechanism from the NPC. There is strong evidence that the discriminatory transport function is mainly the work of the FG-nucleoporins inside the NPC.[9] The name FG nucleoporins is given to these proteins because they have repeated regions of the amino acids phenylalanine (F) and glycine (G) in their amino acid sequence. They are a major component of the NPC and contribute 12 to 20% of the mass of a NPC.[8] Macromolecules that have binding sites for the FG-repeats, can pass through the NPC.[13] These proteins are also called transport factors because they can bind to the cargo that needs to pass from the cytoplasm to the nucleus and then actively transport it through the NPC (or vice versa). Most of these transport factors belong to a family named the karyopherins. Depending on whether they ferry cargo inside or outside of the nucleus, they are divided into the importin and exportin groups respectively. The importins not only have special docking sites that interact with the NPC to mediate the import, but can also bind to proteins that need to transfer to the nucleus. These proteins are tagged with a special sequence of amino acids that designate it as cargo that needs to cross the nuclear membrane.[14] This sequence of amino acids is called the nuclear localization signal (NLS). Exportins also bind to proteins that have a special amino acid sequence, only this time the cargo is tagged with a nuclear export signal (NES). Perhaps the greatest importance of exportins is the export of messenger RNA from the nucleus to the cytoplasm. As its name states, this mRNA transfers the genetic information, contained in the DNA, to the ribosomes, which in turn synthesises proteins from this information.

Let's take a closer look at the specific example of transport through the Saccharomyces cerevisiae's NPC, on which a lot of research has been done. The picture on the title page is a graphical representation of Kap95. The protein's true structure doesn't necessarily have to look like this since there are a lot of different ways in which the protein can bend and form different shapes, all dependent on the environment it is exposed to. Kap95 is short for karyopherin and the number gives the weight of the protein in kDa. Kap95 is an importin for the yeast nucleus. See appendix A for further information on this protein. It is one of 14 importins recognized in yeast cells.[15] This large number of different importins gives rise to a certain level of redundancy. A karyopherin can recognize and mediate transport for more than one single cargo, and also the cargo can be ferried by more than one single type of transport factor. Out of the 14 importins, there are only 4 that are essential in yeast, Kap95 being one of them.

2.3 Models on FG-nucleoporin structures

In Figure 2.1 it is estimated that the FG-repeat regions lie to the centre of the NPC. Yet, the FG-nups are intrinsically disordered proteins (IDP's). This means that the proteins lack a well-defined conformation. They form a disordered region at the walls of the central channel. A lot is still unclear on how this region helps in discriminating between macromolecules and there are a lot of different models that give an explanation on the selective mechanism of the FG-nucleoporins inside the main channel. There are four main models on the structure of FG-nucleoporins in the NPC and the way in which

they regulate transport.[16]

2.3.1 Selective phase model

The selective phase model proposes that the FG-nucleoporins form links with each other through hydrophobic interactions. Figure 2.2 shows that this leads to a sieve-like barrier, in which the mesh size sets the limit for passive exclusion.[17] Transport factors can overcome the size restriction by binding to the hydrophobic clusters of the FG-nucleoporins. This binding competes with the inter FG-repeats cross-links and thus opens up adjacent meshes. Later studies showed that the FG-rich repeat regions in nucleoporins can form hydrogels.[2] For this reason the model is also known as the **hydrogel model**. When the FG-repeats were replaced with other amino acids, this hydrogel could not be formed. This is a strong indication that there is a meshwork of the FG nucleoporins inside the NPC.

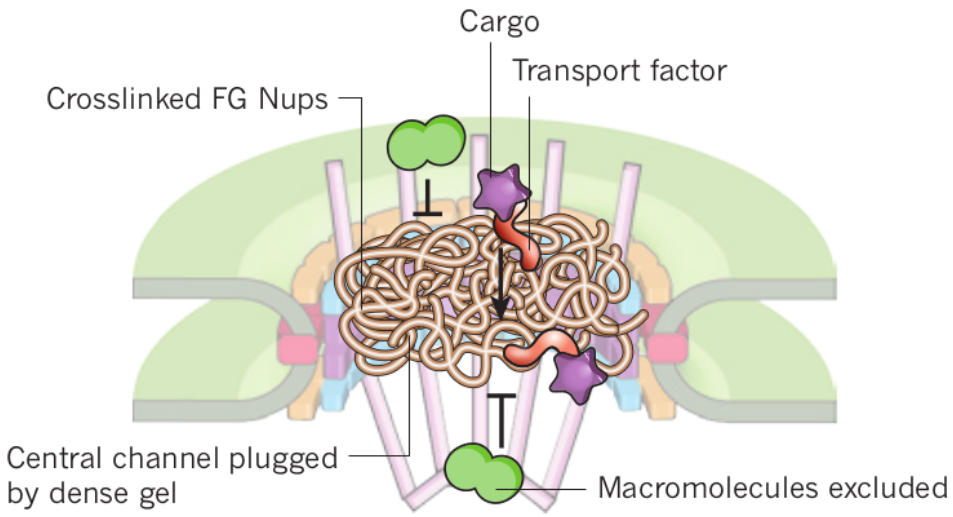

Figure 2.2: The hydrogel model. The transport factors can pass through the FG nups by dissolving the crosslinks.[16]

2.3.2 Reduction-of-dimensionality model

The mechanism of the reduction of dimensionality model can be seen in Figure 2.3. The model claims that the walls of the central channel are lined by a coherent surface of FG-nups.[18] From the entrance of the NPC towards the centre of the central channel there is a build-up of more and more disordered FG-nucleoporins. The selectivity for larger molecules happens because of hydrophobic interactions between the transport factor and FG motifs along the wall of the channel. These binding events give the transport factor a high mobility in the plane of the FG-nups lining and it will slide via a 2D random walk through the channel. Larger macromolecules will be impeded in their translocation through the NPC because they will not be able to interact with the FG-nups on the walls of the NPC.

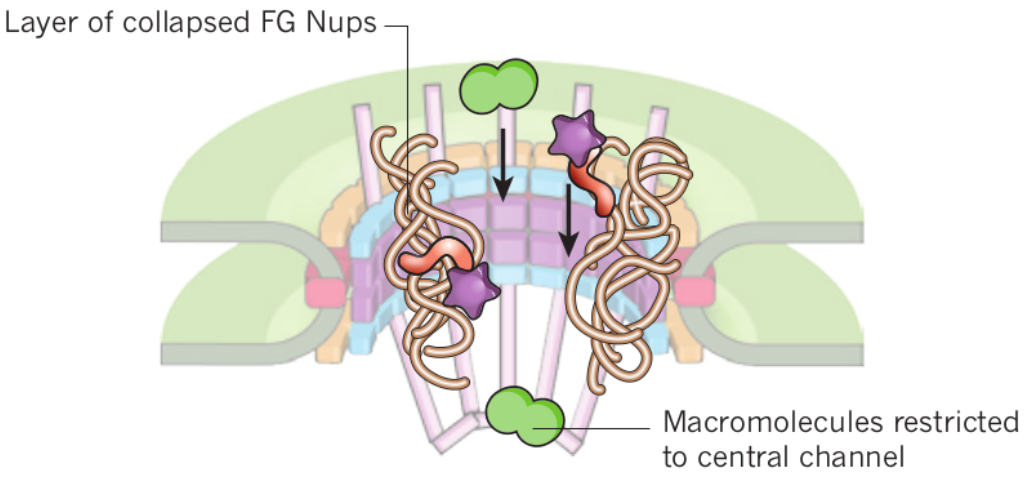

Figure 2.3: The reduction of dimensionality model. Transport factors bind to the FG-nups and then slide through the channel.[16]

2.3.3 Reversible collapse model

The reversible collapse model (which is also called **polymer brush model**) states that when a transport factor is at the entrance of the NPC, the structure of FG-nups slightly collapses inward which grants the transport factor freedom to pass through the NPC. A schematic of this mechanism is depicted in Figure 2.4 . The model came into being to explain the results of experiments caried out by Lim et al.[19] In this research FG-nucleoporins were attached to gold nanodots and then exposed to solutions of differing concentrations of transport factors. For increasing concentrations of transport factor it was observed that the FG-nup height was decreasing which meant that the structure went from a brush like appearance to a more compact, collapsed state.

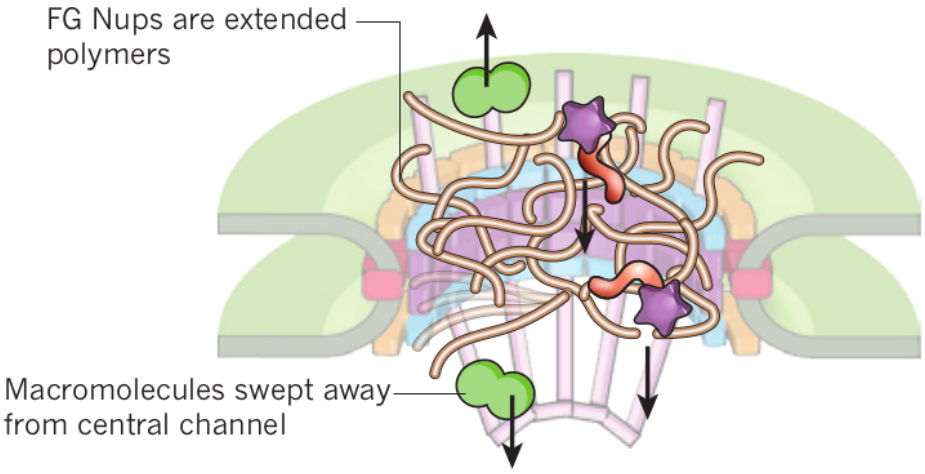

Figure 2.4: The reversible collapse model. The transport factor with cargo collapses the polymer brush like FG-nups.[16]

2.3.4 The virtual gate model

The virtual gate model was formed when Rout et al. examined the composition of a NPC.[20] They found no proteins that are usually associated with mechano-chemical transport. This meant that the function of the NPC had to rely on a more basic mechanism than was previously thought. In this case entropic forces. The virtual gate model suggests that the FG nucleoporins are non-cohesive and are all anchored to the NPC wall. An approximate representation of this model can be found in the schematics of the reduction of dimensionality model (Figure 2.3). Only, instead of the RoD model transport mechanism, the selectivity for the virtual gate model arises because of entropic forces between the transport factor and the FG nucleoporins. When a macromolecule is in the cytoplasm, for example, it has high entropy because it can move virtually freely. When it encounters the nuclear pore though, its degrees of freedom drop drastically and so does its entropy. The walls of the nuclear pore complex are lined with the FG-nups, which further inhibit movement of the transport factor inside the pore. This adds to the entropic price it has to pay. If the size of the macromolecule increases, the entropy of the particle inside the channel becomes lower and lower. The chance that a large macromolecule traverses the NPC becomes negligible because of the low entropy the molecule has to possess. For a transport factor, which has binding sites for the FG-nups, the entropic barrier can be lifted, since it has more degrees of freedom inside the channel through binding events with the FG-nucleoporins. The interactions increase the freedom of the transport factor in contrast to other macromolecule which do not have an affinity with the FG nucleoporins. This mechanism thus facilitates a passage for the transport factor, while blocking other macromolecules.

3. Solid state nanopores

The basic principle of the working of solid state nanopores can be traced back to the Coulter counter, a device used to count and size particles in a fluid. This was a device invented by Wallace Coulter and his brother Joseph in the 1940's to make the cell count in blood easier. It is based on the Coulter principle, also named after the inventors.[21] The functioning of the Coulter counter, and consequently also the solid-state nanopore measurement, boils down to a small hole separating two compartments, both filled with fluid containing electrolytes. One of the chambers also contains the molecules of interest we want to analyze in the fluid. Electrolytes are materials that dissolve in a solvent (e.g. water) and separate into ions. A potential is applied between the two chambers and since the fluid contains electrolytes an ionic current will be created from the charge of the ions that flow through the pore. The current, that is measured, in combination with the applied potential gives the resistance of the hole. The particles in the fluid can also move through the hole (given that the pore diameter is large enough). The transport of particles can be a result of a force on the particle created by an electrical charge on the pore (electro-osmosis) or an electrical charge of the particle itself (electrophoretic force). If there is a concentration gradient over the two sides of the pore, passive diffusion can also cause translocations. When the particle is travelling through the hole, it is blocking the flow of ions. Consequently, a change in current can be observed due to the excluded volume of ions. This change is reflected in the measured current signal and indicates that a particle is moving through the hole. This is known as the Coulter principle.[21] A solid state nanopore is the analogue of the hole in the Coulter counter. As the name implies, it is a pore on the nanometre order in a solid state membrane, such as silicon nitride or graphene. The material being used in this study is silicon nitride. The fabrication of the solid state nanopores is described in a paper by Janssen et al.[22]

3.1 Instrumental setup

An overview of the flowcell with nanopore can be seen in Figure 3.1. There is no functional difference between this modern day setup and the classic Coulter counter from the 1940's, besides the size of the nanopore (pore itself not depicted in Figure 3.1, only the support membrane). To perform a measurement, the nanopore is clamped between the two flowcells. This tight seal is strengthened by the use of rubber O-rings that give a watertight seal and a very high electrical resistance, multiple orders of magnitude larger than the resistance of the nanopore. A buffer solution containing the electrolytes, besides other components, is inserted into the flowcell, effectively immersing the nanopore on both sides. The electrodes are then placed into each flowcell, and a bias voltage is applied to the electrodes by a feedback amplifier, that also measures the ionic current flowing through the nanopore.

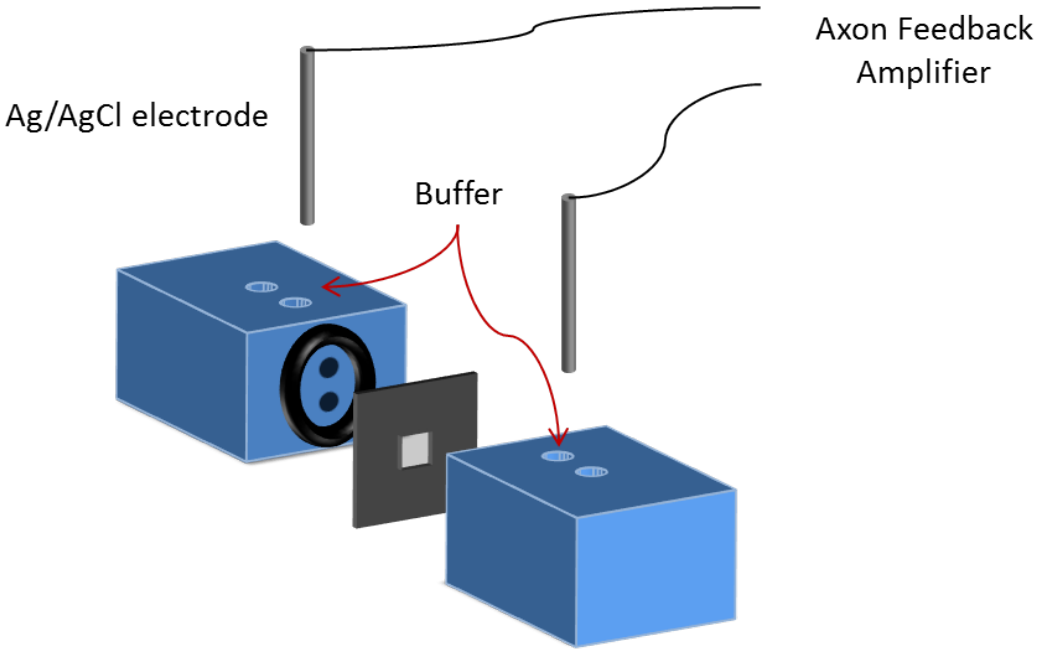

Figure 3.1: Overview of the flowcells (blue blocks) with the nanopore chip. Nanopore chip with supporting Si and SiO_2 layers (dark grey) and free standing SiN membrane (light grey). The entire set is place inside the Faraday cage to shield from external noise. Note: Schematic not to the scale.

3.2 Measurement buffer

The buffer used in the flowcell is of great importance since it not only supplies the ions necessary for a measurable current, but also affects the proteins that we dissolve into the buffer during translocation measurements. The buffer used for all the experiments carried out in this research is composed of the following chemical compounds:

- 150 mM KCl

  The salt concentration is controlled by the amount of potassium chloride (KCl) that is dissolved in the buffer. This disassociates into potassium and chloride ions that are responsible for the current that we measure. KCl is the preferred electrolyte for nanopore sensing experiments for two main reasons. The first advantage KCl offers, is the compatibility with the silver/silverchloride (Ag/AgCl) electrodes. In an ideal case, the potential drop across the nanopore is the same as the bias voltage applied to the electrodes. This potential is influenced by the solution conductivity and by the electrode/solution interface. The use of an Ag/AgCl electrode in contact with an Cl^- containing electrolyte leads to the following reversible electrochemical reaction:

  $$Ag + Cl^- \longleftrightarrow AgCl + e^-$$

  As a result, the combination of KCl with the Ag/AgCl electrodes ensures a fast charge transfer and a high current density exchange at the surface of the electrode. The second advantage of this particular electrolyte is that the ion mobilities of K+

and Cl- are almost the same. Consequently, the two different ion species move at near equal speeds through the solution. If this were not the case, a charge imbalance could result between the two sides of the nanopore, which leads to a non-linear behaviour for voltage differences. Switching the voltage, for example, from 100 mV to -100 mV will lead to different absolute current making it hard to compare measurements.

- 10 mM Tris

  The function of tris (tris(hydroxymethyl)aminomethane) is to act as a pH-buffer. We want to keep the pH around 7.5-7.8 to mimic physiological conditions in the yeast cell as best as possible.

- 1 mM EDTA

  EDTA (ethylenediaminetetraacetic) is a chelating agent. The function of this type of chemical is to bind metal ions in the buffer. The neutralization of these ions is important, because they could attach to the surface of the nanopore and bind the proteins through electrical force. The metal ions can become dissolved in the buffer through dissolution of the surface of the nanopore.

- 1 mM DTT

  DTT (dithiothreitol) is known for its ability to break disulphide bonds. It is important to prevent the proteins, that are dissolved in the buffer, from binding to each other and forming aggregates. The amino acid cysteine, which is abundant in the amino acid sequence of the proteins we analyze, can create a disulphide bond with other cysteine residues. As a result of these bonds the nanopore channel can get clogged due to the size of the aggregated proteins. Furthermore, it would intervene with single protein measurements.

For more details on the materials and methods, see appendix B.

3.3 Conductance of the solid state nanopore

When conducting measurements with solid state nanopores, it is of great use to have a mathematical model describing the transport of ions and other charged species through the nanopore. Not only does this model aid in an understanding of the underlying physics, but it can also be used as a tool to improve measurement accuracy. There are multiple factors which add to the total conductance of the nanopore. In this section only the effects of pore geometry and access resistance on the total conductance will be treated. The effects of surface charge will not be discussed due to its small effect on the conductance and the sophistication of the models.

From the Nernst-Planck equation for ionic flux, the conductance of a simple cylindrical pore with uncharged walls can be deduced.[23] This leads to the following equation for the pore conductance G:

$$G_{pore} = \frac{\pi d^2}{4L} \cdot z_i \cdot F^2 \cdot (u_+ + u_-) \cdot c = \frac{\pi d^2}{4L} \cdot \sigma_s \tag{3.1}$$

In this equation, d and L are the pore diameter and length respectively, z_i stands for the ionic charge, u's are the electrophoretic mobilities of the cation (u_+) and the anion (u_-), F is Faraday's constant and c is the concentration of ions in mol/m^3. The last terms can be shortened to σ_s, the solution conductivity. This simplification can be made because it is assumed that the electrolyte concentration is evenly distributed throughout both flowcells, i.e both sides of the nanopore.

Furthermore, we have to take into account a phenomena called access resistance. This resistance arises because the electric field lines converge from the bulk electrolyte at the entrance of the nanopore. This can be seen in Figure 3.2. A solution for this added resistance was explained by Hall et al.[24]

$$R_{access} = \frac{1}{\sigma_s d} \tag{3.2}$$

This resistance occurs at the entrance of the nanopore, so it can be modelled as being in series with the resistance of the pore channel. This leads to the following result, describing the overall resistance of the nanopore:

$$R_{pore} = R_{acces} + \frac{1}{G_{pore}} = \frac{1}{\sigma_s d} + \frac{4L}{\pi d^2 \sigma_s} \tag{3.3}$$

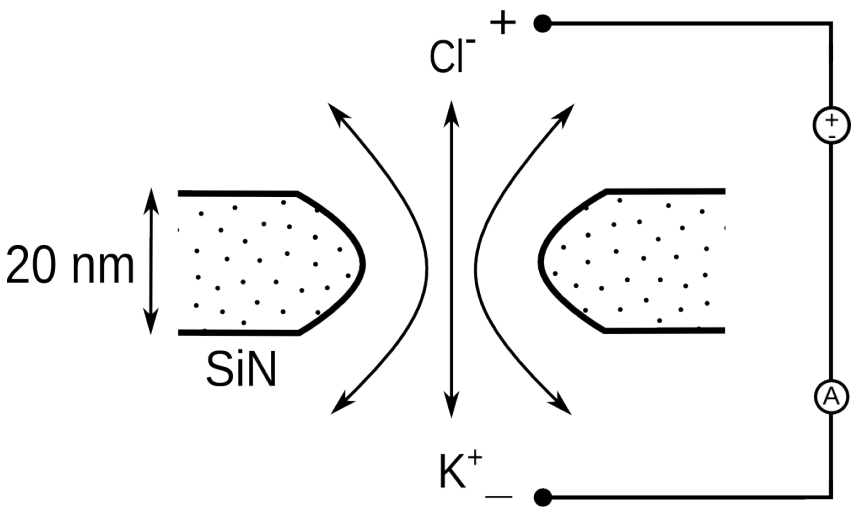

Figure 3.2: Schematic of the hourglass-shaped walls of the nanopore with field lines of the ionic current and applied voltage over the nanopore.

For a concentration of 150 mM KCl at room temperature, the solution conductivity is 1.88 S/m.[25] The fabrication of the solid state nanopore leads to a membrane thickness of 20 nm. The thickness of the membrane being the pore length, L. Conductance measurements have been performed on pores with four different pore diameters, d (20, 40, 50 and 60 nm).

In Figure 3.3 (red line) it can be seen that this model does not fit the measured data properly. The discrepancy with experimental data is mainly caused by the fact that the nanopores used in this project are not perfectly cylindrical. The walls of the nanopore channel are hourglass shaped. This can be noticed in Figure 3.2. The best way to fit

the model to experimental data is by changing the true thickness of the membrane to a so called "effective thickness".[26] The least squares estimator for the effective thickness gives $L = 11$ nm (green line in Figure 3.3). The effective pore length is lower than the true membrane thickness due to the fact that the width at the pore entrance exceeds the diameter at the centre of the pore channel (the value used for the pore diameter, d).

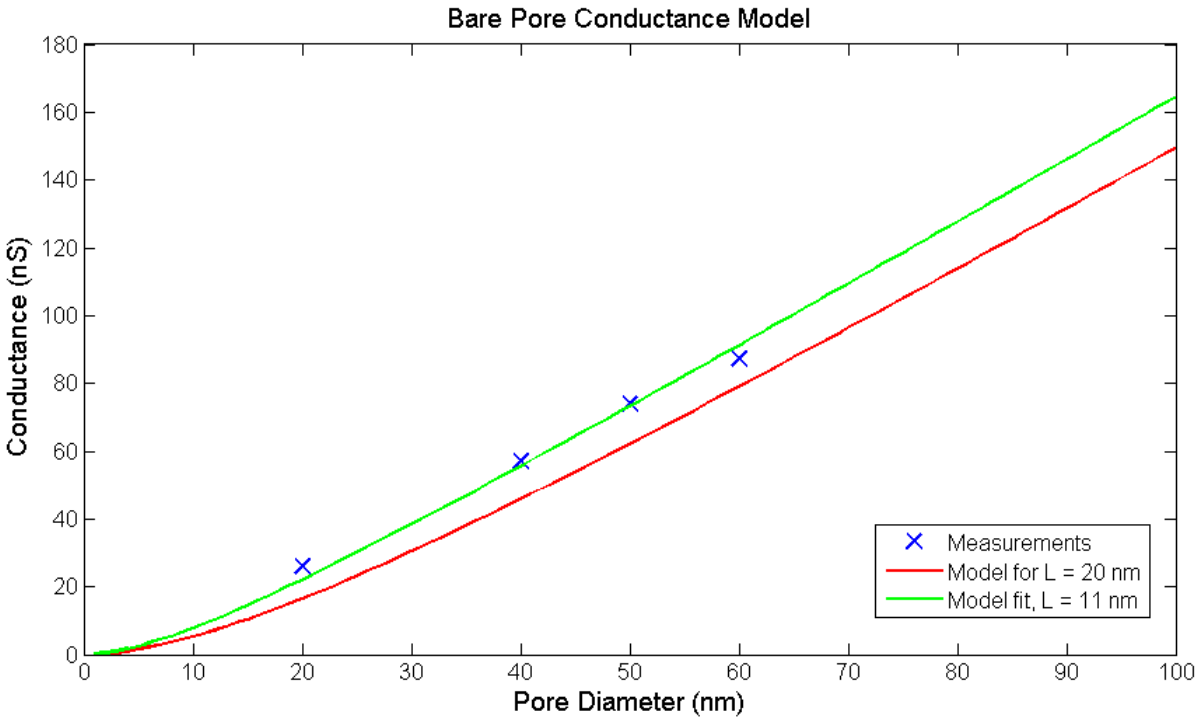

Figure 3.3: Measured bare pore conductance with fitted model based on equation 2.3.

3.4 Protein translocation

In a protein translocation experiment, the nanopore is flushed on both sides by the measurement buffer. When an potential difference is applied between both side of the nanopore, the ions will flow through the nanopore, creating an ionic current. Proteins can be electrically charged, depending on the environment they are exposed to. If the protein is in an aqueous solution, such as our buffer, its electric charge will be mostly dependent on the pH value of the solution. At a certain pH value the protein will not carry a net electric charge, called the isoelectric point (pI). If the pH value of the solution rises above the proteins pI value, the protein will carry a negative charge. For a solution pH value that lies below the proteins pI value, the protein becomes positively charged. If the protein is added to the buffer on one side of the flowcell, it can then become a charged species. Under the influence of electrophoretic and electro-osmotic forces the protein can translocate through the nanopore, causing a disturbance in the flow of ions. Consequently, the change in electric current can be measured, which is the basis for nanopore sensing. In Figure 3.4 a typical protein translocation event can be seen. The current is decreased when the protein is moving through the nanopore because it is occupying space from the

flow of ions. The time it takes from entering the pore and exiting on the other side, is called the dwell time. The drop in current caused by the translocating protein is called the conductance blockade.

In this study two proteins will be used for translocation, kap95 and tCherry. The measurement buffer we use will cause kap95 to be negatively charged and tCherry will carry a positive net charge. Further information on the proteins can be found in Appendix A.

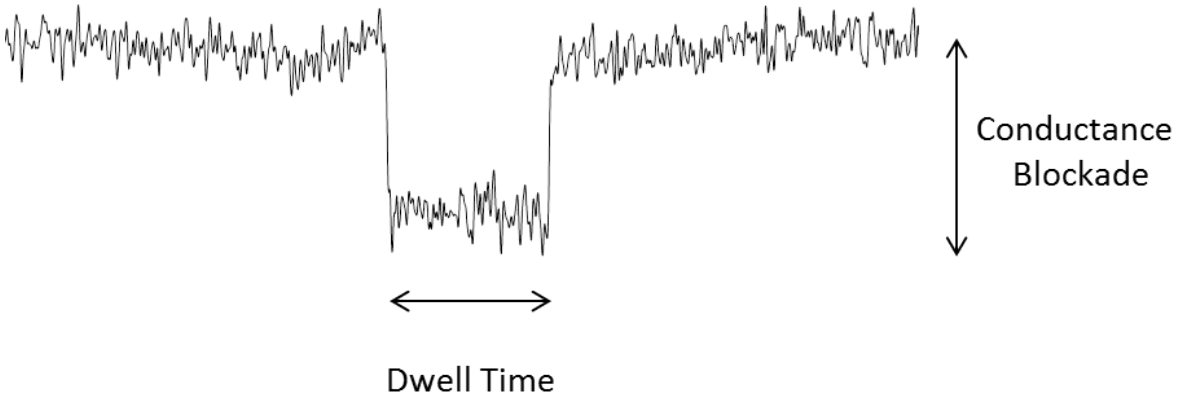

Figure 3.4: Example of a translocation event in a current trace. This particular trace has a length of 10 ms and the current blockade is around 25 pA.

3.5 Noise reduction and data filtering

As we are working with a low salt concentration, it is hard to detect translocation events due to the low conductance through the nanopore. The low salt concentration is inherent to the project, as we are trying to maintain physiological conditions. With lower conductance it is inevitable to suffer from a decrease in signal-to-noise ratio. There are two tools at our disposal to still gain useful data. The first method is applying a low pass filter to the data. The second tool involves physically modifying the solid-state nanopore in such a way as to decrease noise.

The filter is applied in the software used to analyze the raw data from the measurements. All the data in this report is filtered with a Gaussian low pass filter with cutoff frequency at 5 kHz.[27] The effect of applying such a filter is that the high frequency noise is suppressed and that translocations can be analyzed with much greater ease.

The noise sources in solid-state nanopore measurements are diverse. There are two main contributors to the overall noise of the nanopores. The first noise source is high frequency background noise originating from the capacitance of the silicon nitride membrane on the support chip.[28] The second noise source is a low frequency flicker noise originating from measurement equipment. Fortunately, there is a way to reduce these noise sources dramatically by coating the membrane side of the nanopore with PDMS (polydimethylsiloxane). The coating was done under a microscope, in which a small drop of PDMS was spread out across the support chip with a needle, carefully avoiding the free standing membrane with the nanopore. The PDMS was cured onto the chip by baking

in the oven for 30 minutes at 100°C. The noise reduction is clearly visible in a current trace such as in Figure 3.5. Without PDMS curing the translocation events in a bare pore would get drowned in the background noise. All the data in this report is acquired from measurements carried out with PDMS coated solid-state nanopores.

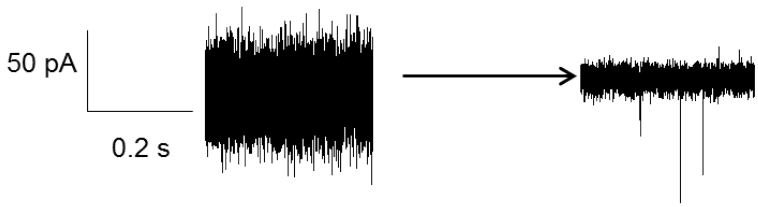

Figure 3.5: A current trace with translocation events. Before PDMS coating the translocations can't be detected, and after PDMS coating they are clearly seen in the current trace.

4. Biomimetic nanopores

Nature has always been a source of inspiration to scientists. A great example would be Leonardo da Vinci who studied birds and tried to engineer a machine resembling their wings to facilitate flight. Unfortunately though, he failed. Yet his research paved the way for future ideas on aviation. Another great idea that was borrowed from nature, is the honeycomb structure that bees use in their hives. The hexagonal structure is an ideal combination of strength and a minimal amount of materials needed, and for this reason it can be found in aircraft wings, elevators and floors. Even the solid state nanopore, introduced in the previous chapter, has biological roots. When the idea was proposed that DNA could be sequenced by threading the strand through a nanopore, research into biosensing with nanopores was born.[29] During the first stage of research into this new field, scientist looked towards nature and found a lot of nanopores in biology they could use for their experiments. There is a broad range of biological nanopores, from proteins that form nanoscale channels in lipid bilayers to ion channels. Soon though it was realized that the biological nanopore had limits and the rise of solid state nanopores began. The synthetic nanopore in a solid-state material had multiple advantages over its biological counterpart. For example, the biological nanopore was very sensitive to pH values and voltages, whereas the solid state nanopore was more robust and could be deployed over a much broader range of environment variables. Also, the size of biological nanopores could not be changed, whereas the diameter of the solid-state nanopore can be easily manipulated. Over the last decade a lot of progress has been made with solid-state nanopore sensing.

Besides DNA translocation studies, which are still the major focus of nanopore research, other areas are being given an increasing amount of attention. One of the new applications of solid-state nanopores is towards protein analysis by surface modification of the solid-state nanopore. By modifying its surface, a broad range of functions can be given to a solid state nanopore. In this research we will modify the surface of a solid state nanopore as to replicate a basic version of a nuclear pore complex. This biomimetic nanopore is an artificial copy of the real nuclear pore complex in a cell. First we will explain the use and function of the biomimetic nanopore. Afterwards, the method for the surface modification and the conformation of proteins to which this lead will be discussed.

4.1 Function and use of a biomimetic nanopore

In chapter 1 the function and mechanism of a NPC was explained. Since the NPC is the only connection between the nucleus and cytosol of eukaryotic cells, it plays a vital role as gatekeeper. To fulfill this role, the NPC has a selective function. How the NPC can maintain this discriminatory feature is not fully understood yet.

By mimicking the NPC we can achieve two important goals.

- To understand how the NPC works. In chapter 1.3 many different models were discussed on how the NPC might function. At the moment there is a great deal

of uncertainty surrounding the discussion on which of the models are right. By creating a replica of the NPC we might be able to find out which model fits the experimental data best.

- To use the selective feature for many practical applications. The NPC only grants passage to and from the nucleus to certain proteins, which is a very powerful feature. It has been shown that a membrane with many nanopores coated with FG-repeat nucleoporins exhibits transport selectivity for proteins.[30] We can find many uses for this new type of nanopore. For example, we can deploy the biomimetic nanopore for purification purposes. If a protein or macromolecule of interest is suspended in a crude mixture of proteins, a biomimetic nanopore can be used to extract only these molecules. Also, an increased understanding of the workings of a NPC can aid in the creation of medicine which target this part of the cell. If we coat a single nanopore with nucleoporins, as in this research, we can obtain more detailed information on the interaction between translocating proteins and the nucleoporins.

In this research we will try to shed some light on the role of FG-nucleoporins. We will mimic a NPC with FG-nucleoporins and test the selectivity of this nanopore. After the FG-coated nanopore is tested, we will use mutated nucleoporins which lack the FG-repeat regions. We will test the selectivity of the mimicked NPC with the mutated nucleoporins. Should there be no discriminatory function, then we have strong evidence that the FG-regions of nucleoporins are responsible for the 'gatekeeper' function of an NPC.

4.2 Surface modification of solid-state nanopore

To create a biomimetic nanopore we start out with a solid-state nanopore. The chip has been treated with PDMS as described in chapter 2.6. To functionalize the solid-state nanopore, a three-step process is carried out. In the first two steps chemical modification of the nanopore surface is carried out to facilitate the attachment of nucleoporins, which is covalently bound to the modified surface in the last step. In this section we will explain how the surface is modified. In the next section the possible complications that might arise during the modification will be discussed.

In Figure 4.1 the chemicals and nucleoporin, which are involved in the three step surface modification process, are depicted. Before we begin with the surface modification the solid-state nanopore is cleaned with H_2O, ethanol and blow dried with N_2. The chip is then immediately placed in a oxygen plasma chamber for 30 seconds to remove organic impurities and make the surface hydrophilic.

1. APTES silanization

   Figure 4.1.1 depicts APTES. In a process called silanization, this chemical is attached to the siliconoxide surface. The nanopore is placed in an eppendorf with methanol with 5% volume APTES. The total solution volume is 1 mL. The nanopore in solution is placed in a shaker at room temperature at 300 RPM. After one hour the nanopore is taken out of the APTES solution and placed in an vial with pure methanol for 10 minutes. During the 10 minutes the nanopore is also placed in the shaker at 300 RPM to ensure that excess APTES is washed off. The nanopore chip

is then blow dried with N_2. The chip is heated in a oven at 100°C for one hour to perform hydrolysis of the APTES covered surface.[31] This first step leads to the creation of primary amines on the surface.

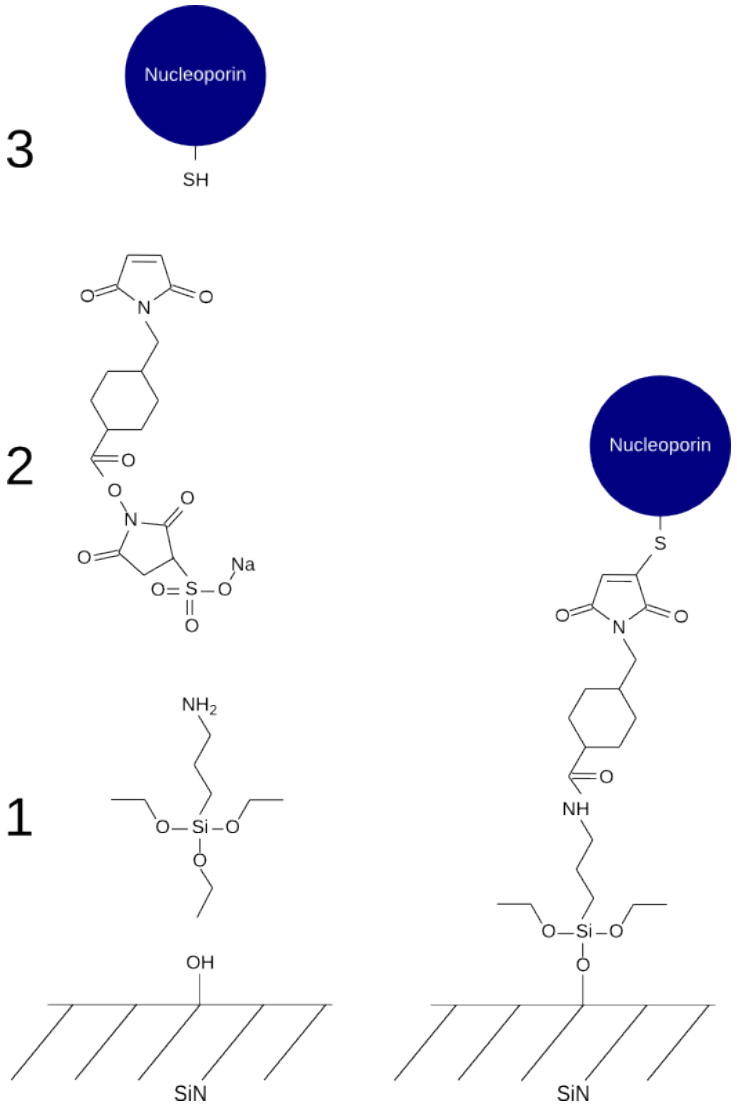

Figure 4.1: Surface modification of the solid-state nanopore to attach nucleoporins. 1 - APTES, 2 - sulfo-SMCC, 3 - nucleoporin.

2. Sulfo-SMCC

   Figure 4.1.2 depicts sulfo-SMCC, an amine-to-sulfhydryl crosslinker (Thermo Fisher Scientific, 2 mg weight capsule). The weight capsule is dissolved in 1.5 mL PBS by shaking vigorously and heating up to 60°C to accelerate the dissolving process. A single nanopore is incubated in 0.5 mL of the sulfo-SMCC solution. The nanopore is shaked at 300 RPM, room temperature and overnight. The chip is then washed with Milli-Q water, ethanol and Milli-Q again, to rinse off excess sulfo-SMCC.

3. Nucleoporin attachment

   The nucleoporins used in this research are yeast Nsp1 wild-type (FG-nucleoporin for short) and Nsp1-FILV → S mutated (SG-nucleoporin). For both proteins the steps are essentially the same, except incubation time. The nucleoporins were stored in 7.3 M guanine HCl in -80°C. The buffer exchange process was carried out as follows:

   (a) 10 µL of 75 µM Nsp1-WT or 5 µL of 80 µM Nsp1-FILV → S is taken from the -80°C freezer and divided over two 30 kDa filtration vials with 500 µL PBS each.

   (b) The filtration vials are centrifuged at 10.000 RPM for 8 minutes.

   (c) Excess PBS is removed from the collector vial and 500 µL of PBS is added to the filtered nucleoporin.

   (d) Repeat steps b and c twice.

   (e) The filter is placed upside down in a new collector vial and spinned at 5.000 RPM for 3 minutes.

   The guanine HCl buffer should now completely be replaced with PBS.[32]

   Before we incubate the chip in a vial with the nucleoporins, we need to prevent that the nucleoporins form disulphide bonds with each other.

   (f) We add together:

   - 40 µL of the Nsp1 WT or 75 µL of Nsp1-FILV → S in PBS buffer
   - 1 µL of 500 mM TCEP
   - 459 µL of PBS for Nsp1-WT or 424 µL of PBS for Nsp1-FILV → S

   This leads to a final concentration of 120 nM nucleoporin.

   (g) Let the TCEP reaction happen for 30 minutes.

   (h) Place a chip that has been treated with the crosslinker, in the vial. The incubation time for Nsp1-WT is 45 minutes and for Nsp1-FILV → S 20 minutes.

   (i) Take the chip out and store in PBS. Now we can run a measurement or keep the coated nanopore stored at 8°C.

4.3 Models for the nucleoporin structure inside the biomimetic nanopore

The true conformation of the nucleoporins on the surface of the solid-state nanopore is hard to determine with accuracy. All we know with certainty is that the nucleoporins are deposited onto the surface through a disulhpide covalent bond with the crosslinker. In Figure 4.2 images acquired with a transmission electron microscope of a 50 nm solid state nanopore can be seen. The left side shows a bare pore and the right is the same pore after coating with FG-nucleoporins. We can observe that a material is covering the nanopore, which is most likely the nucleoporin.

Research from Eisele et al[33] in which the same nucleoporins were used as in our experiments, suggests that the FG-domains in nucleoporins interact attractively with

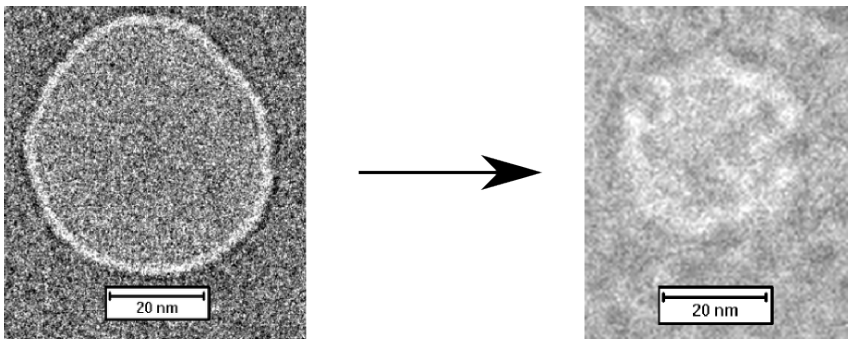

Figure 4.2: TEM images of a 50 nm bare solid state nanopore (left) and a nanopore after FG coating (right).

each other. The nucleoporins can form a layer when deposited on a surface because of the cohesive interactions. However when the wild-type nucleoporin was mutated by replacing the hydrophibic patches by serine, it was found that the cohesiveness of the nucleoporin layer drastically reduced. So the layer thickness is dependent on nucleoporin type and concentration, and incubation time. In our experiments one of the greatest challenges was to find the precise balance between incubation concentration and time for the nucleoporin attachment to the solid-state nanopore surface. We kept the incubation concentration constant at 120 nM and tweaked the incubation time.

A schematic can be seen of a nanopore with attached nucleoporins on the surface in Figure 4.3. Due to a low incubation time the nucleoporins have formed a thin layer. For FG-coating a low incubation time would be around 15 minutes. A macromolecule (such as kap95 or tCherry in our case) that translocates through the nanopore can do so without interacting with the nucleoporins due to the large amount of space in the pore that is not taken up by the nucleoporins.

Figure 4.3: Schematic representation of a nanopore coated with nuceloporins (blue). The low incubation time leads to a very thin layer of nucleoporins.

On the other hand a high incubation time gives rise to a new problem. It can be seen in Figure 4.4 that the nanopore is completely filled with the nucleoporins. If the pore is filled with nucleoporins, we can't measure a conductance blockade since the ionic conductivity drops to nearly 0 nS. A protein that translocates through the nanopore can do so without being detected since there is no current blockade to be observed.

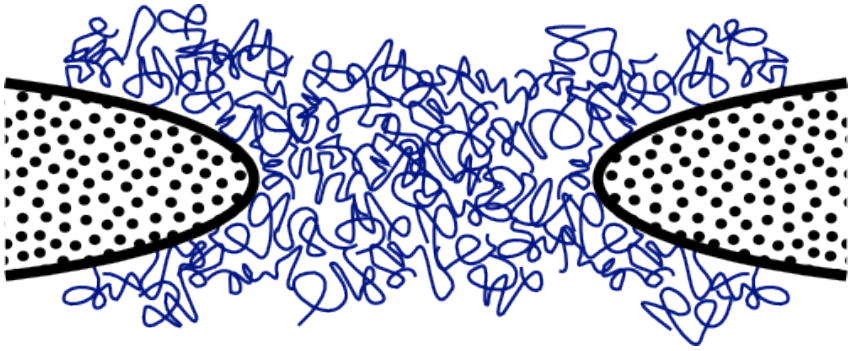

Figure 4.4: Schematic representation of a nanopore coated with nucleoporins (blue). Higher incubation times leads to clogged nanopore.

The best scenario can be seen in Figure 4.5. In this schematic it is shown that with the right incubation time a nucleoporin layer can be formed on the nanopore with a thickness that leaves enough room in the centre of the pore. If a protein would translocate through the pore a current blockade can be detected. Also the protein can only translocate if it interacts with the nucleoporins. In the case of SG-coating though, a layer as seen in Figure 4.3 is more likely due to the previously mentioned lack of cohesiveness.

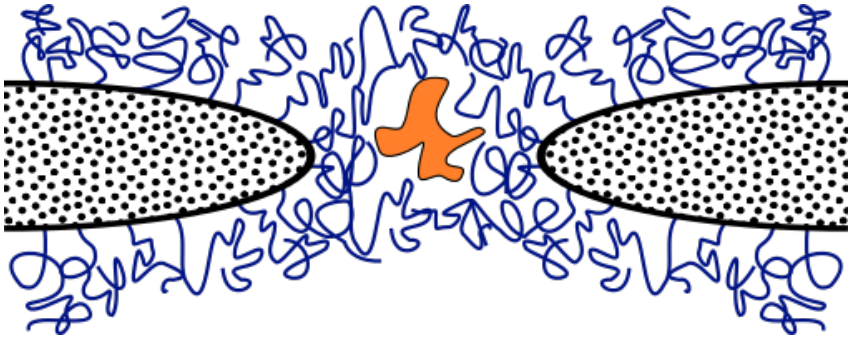

Figure 4.5: Schematic representation of a nanopore coated with nucleoporins (blue). In an ideal situation the nucleoporins form a layer that is just thick enough so a clear current blockade can be seen if a protein (orange) translocates through the nanopore.

5. Results and Discussion

We present the results from our protein translocation experiments in this chapter. In the first section we will explore the translocations of two proteins, kap95 and tCherry through a bare pore. In sections 5.2 and 5.3 we will discuss the translocations of the same proteins through pores coated with nucleoporins. In the final section, we will discuss the frequency at which the proteins translocate through the different kind of pores. The concentration of the translocating protein is 100 nM, unless noted otherwise.

5.1 Bare Pore

5.1.1 Kap95 through a bare pore

The first experiments carried out was the translocating of kap95 through a bare pore. In Figure 5.1 the dwell times can be seen of kap95 translocating through a bare pore (amount of events n = 1912). About 13% of the detected events have dwell times higher than 5 ms and are most likely sticking events in which the protein temporarily gets stuck on the sides of the nanopore.[34] After fitting a log-normal distribution to the histogram, we can find the global maximum of the probability density function and a 95% confidence interval for the fitting parameters, as can be seen in the figure as well. The most likely dwell time is **0.17 ms**.

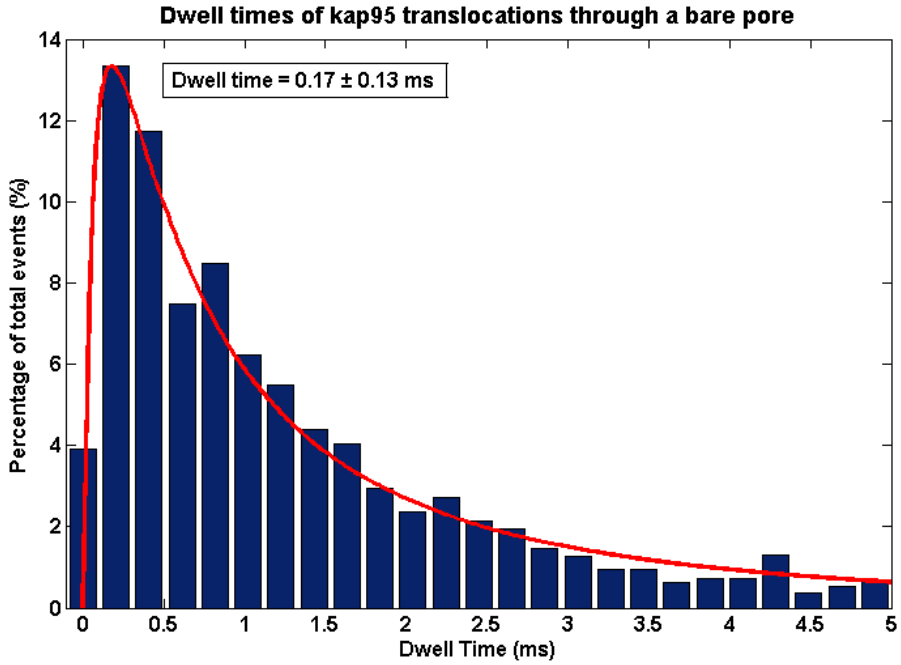

Figure 5.1: Histogram and log-normal fit of dwell times of kap95 translocating through a bare pore (n=1912). The mode of the log-normal fit is 0.17 ms. The bin width is 0.2 ms.

The next data we present is the conductance blockade caused by the translocating kap95. In Figure 5.2 the histogram can be seen of conductance blockades caused by every translocation event we have detected. It is difficult to find a proper fit for a histogram of conductance blockade due to its shape that is different for each protein. For kap95 a log-normal distribution would come to mind first, but as we will see in a moment, this distribution does not properly fit for tCherry conductance blockades. To maintain consistency, no distribution will be fitted over the conductance blockade histograms. The most likely conductance blockade in Figure 5.2 is **0.15 nS**.

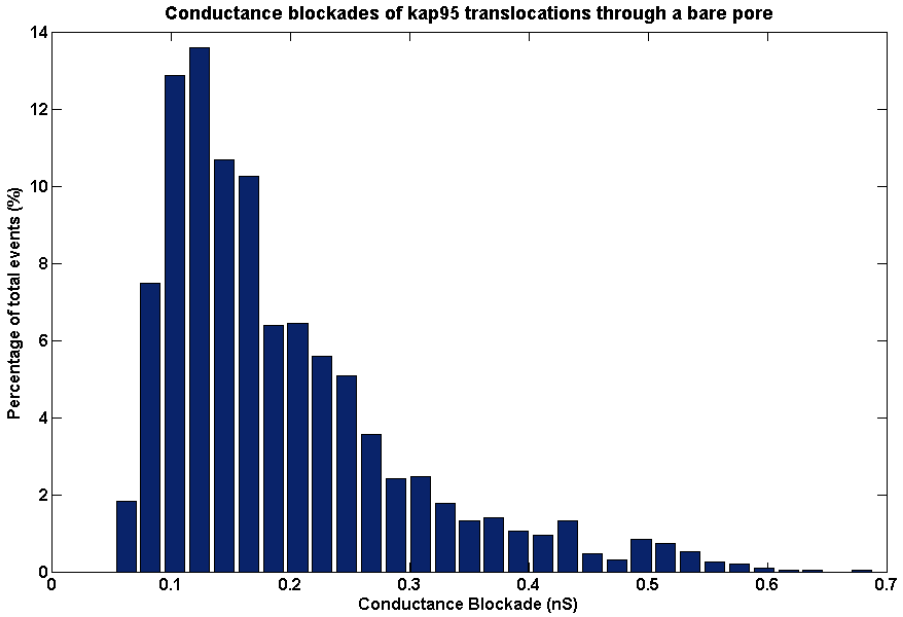

Figure 5.2: Histogram of conductance blockades of kap95 translocating through a bare pore (n=1912). The most likely conductance blockade is 0.15 nS. The bin width is 0.02 nS.

5.1.2 tCherry through a bare pore

The second protein we translocated through a bare pore is tCherry, which served as our control protein. tCherry is a tetramer of the most widely used red florescent protein, mCherry. In Figure 5.3 the dwell times of tCherry translocating through a bare pore can be seen (n=2829). About 6% of the detected events have dwell times higher than 2 ms and are thus not depicted. A quick comparison with the dwell times of kap95 show that tCherry translocates a lot faster through the bare pore. The dwell time is in fact so short that the equipment is being pushed to its detection limit. With a 5kHz filter, which is applied to all the analyzed data, we are able to detect events with a dwell time of 133 microseconds or more with accuracy. Any event that we detect which has a dwell time below this threshold is distorted. As can be seen in Figure 5.3 the largest part of detected events have a dwell time of **0.1 ms**. This means that the events with an even lower dwell time are undetected due to the limit of the signal to noise ratio.[34] We can hypothesize that the shorter dwell time of tCherry is caused by the hydrophilic nature of the protein. Whereas kap95 has hydrophobic patches and sometimes get stuck momentarily on the

pore walls, tCherry does not stick to the side walls, thus translocates quickly through the pore.

The conductance blockade caused by the translocating tCherry, is depicted in Figure 5.4. Not only does the dwell time of tCherry differ greatly from kap95, also the conductance blockade histogram shape varies. In this case the histogram resembles a normal distribution. The most likely conductance blockade is **0.30 nS**.

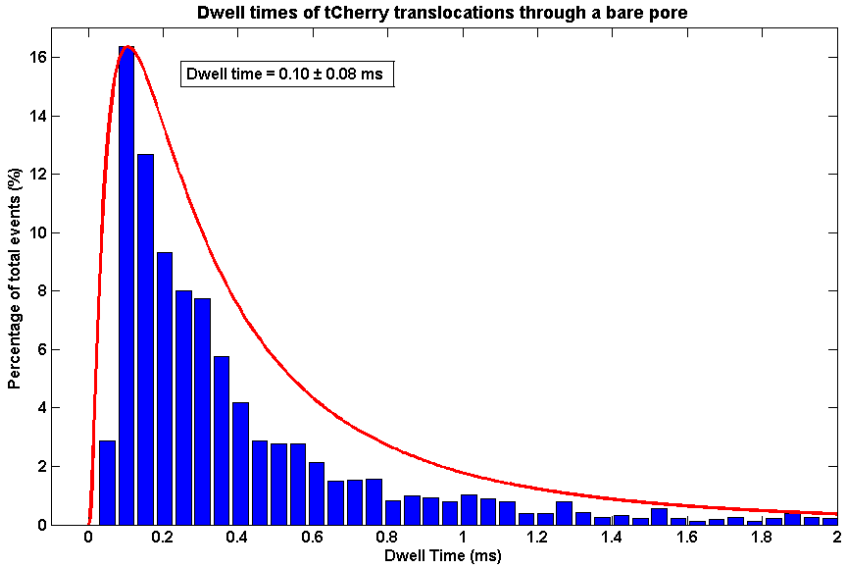

Figure 5.3: Histogram and log-normal fit of dwell times of tCherry translocating through a bare pore (n=2829). The mode of the log-normal fit is 0.10 ms. The bin width is 0.05 ms.

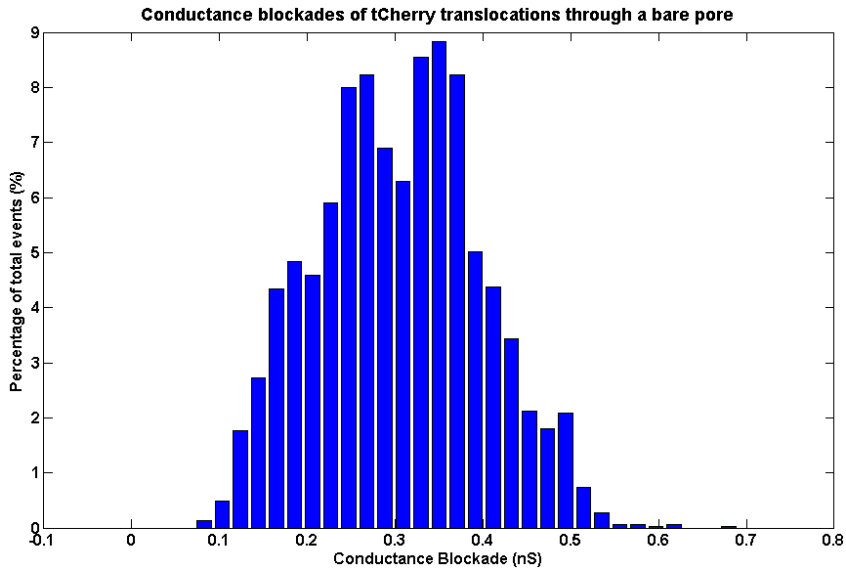

Figure 5.4: Histogram of conductance blockades of tCherry translocating through a bare pore (n=2829). The most likely conductance blockade is around 0.30 nS. The bin width is 0.02 nS.

5.2 FG-nucleoporins coated pore

After the bare pore experiments were done, we started to coat the nanopores with the FG-nucleoporin, Nsp1-WT (FG-coated pore, for short). The procedure for coating was explained in chapter 3.2. After coating the pore, the conductance dropped since a portion of the pore is now occupied with nucleoporins. In Figure 5.5 the difference in current can be seen between a bare pore and an FG coated pore at different voltages. From the IV-plot we can derive that the FG coated pore has about 80% less conductance than the coated pore. It is important to note that the FG-coated pore has linear IV behaviour, so increasing the voltage up to 200 mV does not significantly affect the FG-coating. If the current would increase non-linearly for increasing voltages this would indicate that the nucleoporins are detaching from the surface or aligning in a different way. From the linear IV it is also clear that ions can freely pass through FG-coated pores without affecting the biomimetic nanopore.

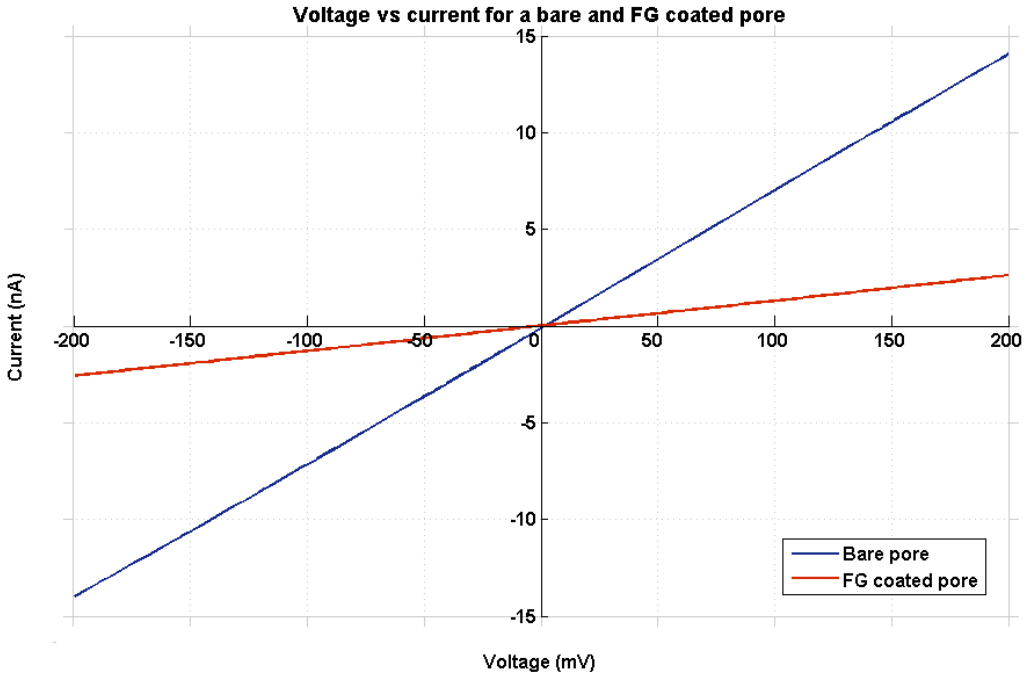

Figure 5.5: IV-curves of a 50 nm pore before and after FG coating.

5.2.1 Kap95 translocations through a FG coated pore

As expected, we saw clear interactions between the kap95 and a FG coated nanopore. Interesting to note is the behaviour observed over time after exposing the nanopore to a buffer with kap95. Two current traces are shown in Figure 5.6, obtained after adding 100 nM kap95 into the buffer. The left current trace is 5 seconds after introducing kap95 into the buffer. We see conductance blockades, same as with a bare pore. Most noteworthy is the increased event frequency in the FG coated pore compared to a bare pore. In the bare pore, we had an average of 10 events per second, whereas in the FG coated pore we found around 25 events per second in the beginning of the measurement. The right current

trace in Figure 5.6 is obtained 2 minutes later than the left trace. After waiting some time, we have an event frequency that matches the bare pore kap95 translocations. We observed the same pattern with an SG coated pore and will discuss this behaviour further in chapter 5.4. The main problem is that we observe conductance increase events. This was highly unexpected. A look at the baseline finally gave us the answer to this weird phenomena. The conductance increase spikes are at a current level that matches the baseline current, the current observed before we inserted kap95. So the upward spikes in the current trace are not translocation events, but the baseline current. The translocation events happen between the conductance increase spikes.

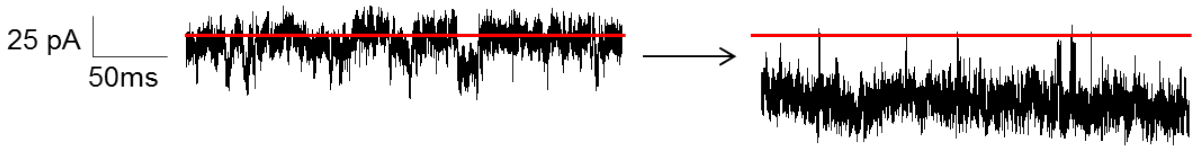

Figure 5.6: The left current trace is 5 seconds after adding kap95 to the measurement buffer. Right trace is taken 2 minutes after the left trace. The red line approximates the baseline or the open pore current level of the FG-coated pore.

In Figure 5.7 the dwell times of the kap95 translocation events can be seen (n=552). If we fit a log-normal distribution over the dwell time histogram, we find that the most likely dwell time is around the **5 ms**, although almost 50% of the events have translocation times higher than 50 ms. This is a dramatic difference in dwell times compared to the bare pore.
The dwell time histogram shows a wide range of dwell times, the highest dwell time recorded was around 600 ms. These events are in the tail of the distribution, as was the case for our bare pore experiments.

In Figure 5.8 the conductance blockade of the translocating kap95 can be seen. The most likely conductance blockade is **0.16 nS**, which coincides with the conductance blockade levels of kap95 translocating through a bare pore. Furthermore the shape of the conductance blockade histogram matches that for the bare pore kap95 translocations as well. Both these observations make a strong case that the events we detected are indeed kap95 translocations, based on the volume exclusion models for protein translocation.[35]
To further compare the kap95 translocations through a FG coated pore and bare pore, the events are coplotted in Figure 5.9.

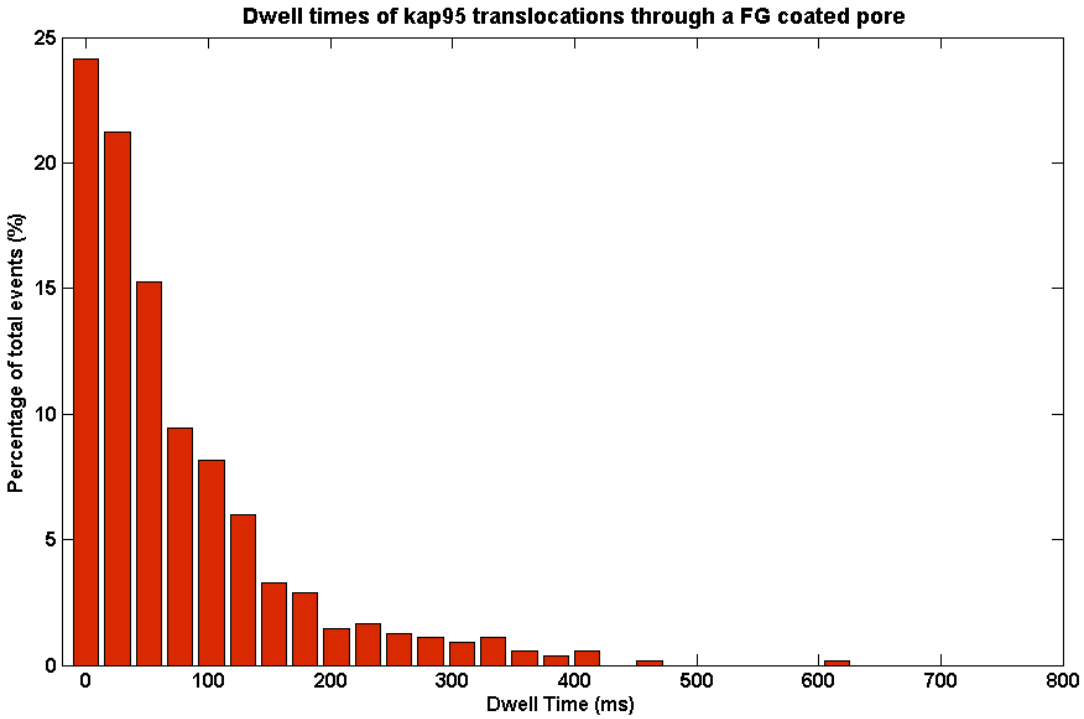

Figure 5.7: Histogram of dwell times of kap95 translocating through a FG coated pore (n=552). The largest peak is around 5 ms. The bin width is 25 ms.

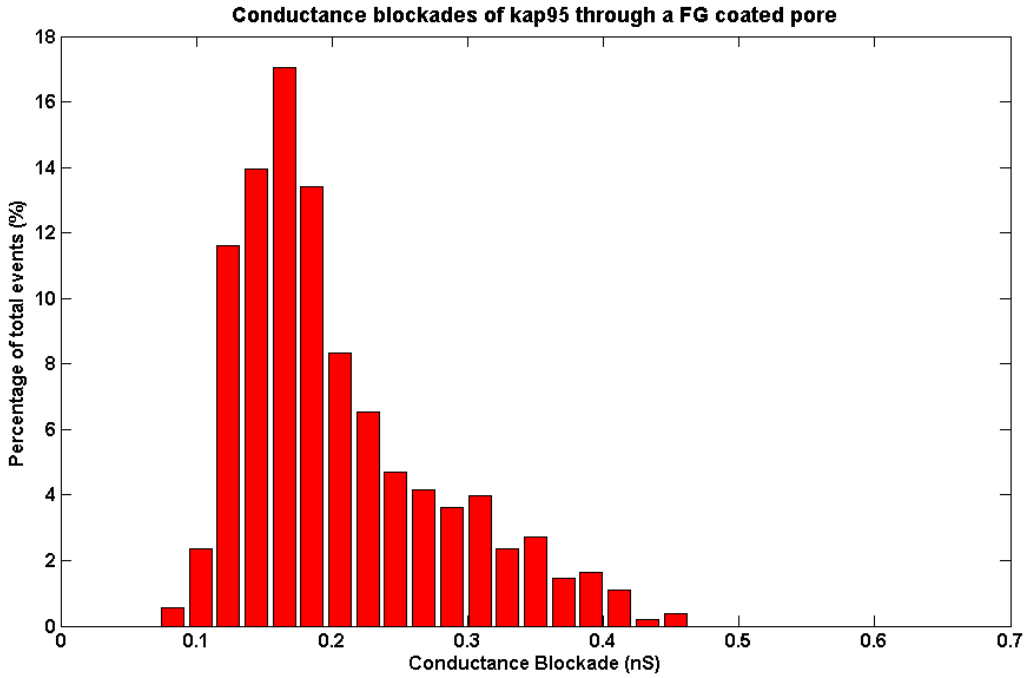

Figure 5.8: Histogram of conductance blockades of kap95 translocating through a FG coated pore (n=552). The highest bar is at 0.16 nS. The bin width is 0.02 nS.

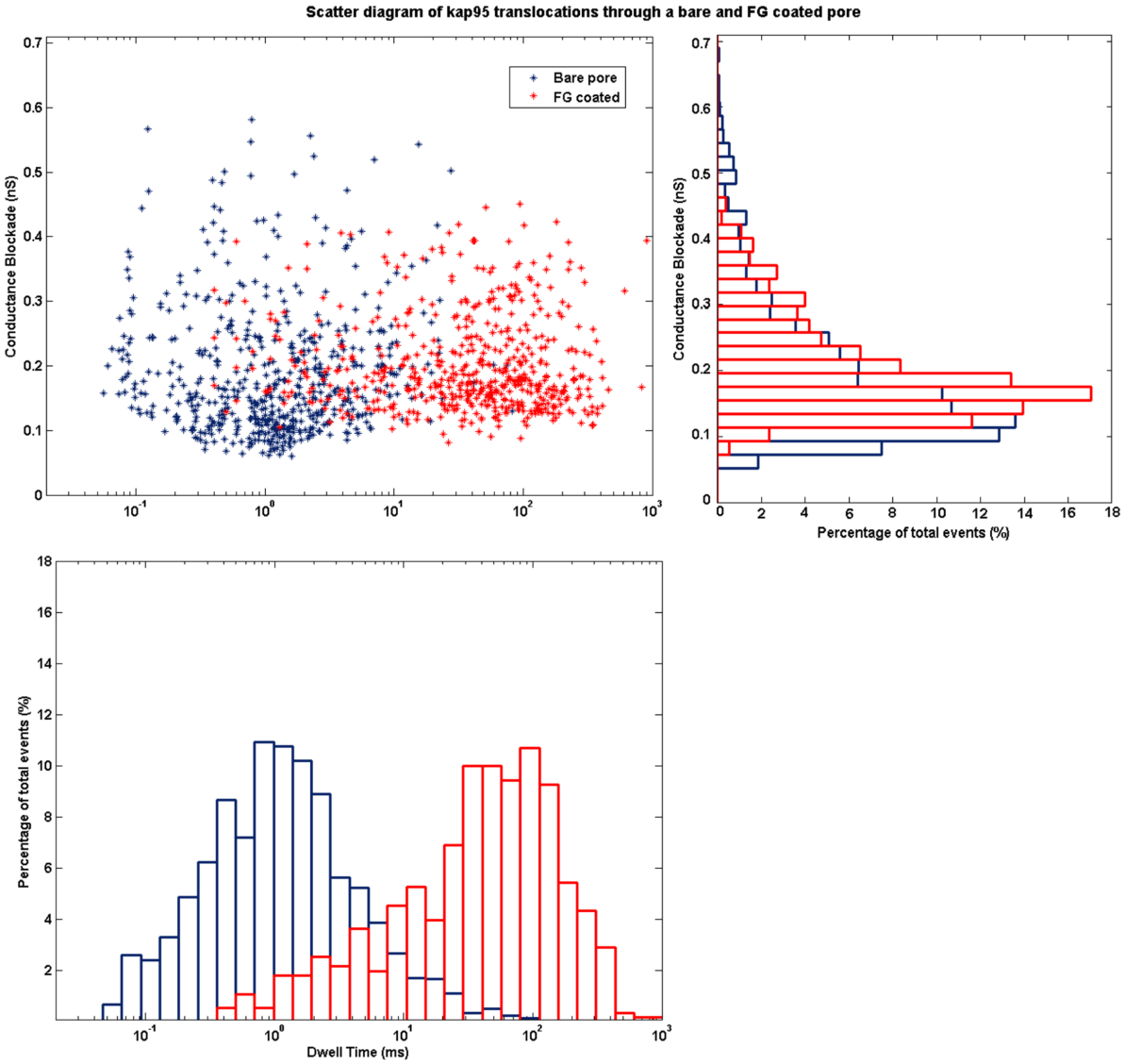

Figure 5.9: Scatter plot for comparing the dwell times and conductance blockades of kap95 translocation events through a bare and FG coated pore.

5.2.2 tCherry translocations through a FG coated pore

After the successful kap95 translocations through our FG coated pore, we tested if tCherry would also translocate. After measuring for over 30 minutes on three different FG-coated pores, we were not able to detect a single event, which is what we expected to happen. Apparently tCherry can't translocate through the FG coated nanopore due to the discriminatory function of the biomimetic nanopore.

5.3 Mutated FG (SG) nucleoporins coated pore

After observing the discriminatory function of the FG coated pore, we set out to test if a mutated version of Nsp1-WT will have the same effect. We use a Nsp1-FILV $\rightarrow$ S mutation, as mentioned earlier, to coat a nanopore. Figure 5.10 shows the IV-plots of a nanopore before and after SG coating. The SG-coated pore has about 50% less conductance than the bare pore. The conductance of the SG coated pore is higher than that of the FG-coated pore. The difference in conductance can be explained by a difference in nucleoporin arrangement on the nanopore surface. As mentioned in Chapter 4.3, the mutated FG nucleoporin lacks the ability to form compact cross links. In this case the structure of nucleoporins will most likely look the schematic of Figure 4.3. Since there is more space inside the pore unoccupied by nucleoporins, the conductance is higher. As with the FG coated nanopore, the SG coated pore exhibits linear IV behaviour which indicates that higher voltages don't affect the SG nucleoporins as more and more ions go through the coated pore.

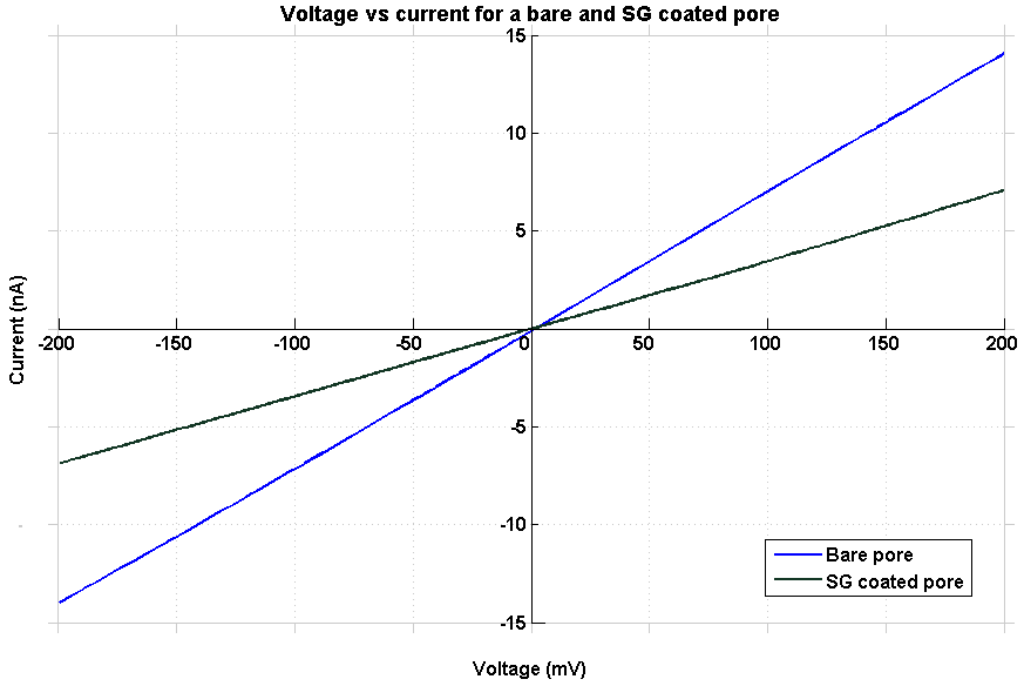

Figure 5.10: IV-curves of a 50 nm pore before and after SG coating.

5.3.1 Kap95 translocations through a SG coated pore

In Figure 5.11 we can see the current traces of a measurement with a SG coated pore. Right after adding kap95 into the buffer an event frequency of 30 Hz can be observed. After a while though this drops down to the normal level of kap95 through a bare pore, around 5 Hz. With the FG coated pore, the same drop over time in event frequency was observed. A theory on this strange behaviour is given in chapter 5.4.

Figure 5.11: Left current trace is immediately after kap95 insert. Right trace is taken 10 minutes after the left trace. There is a drop in event frequency between the traces.

The dwell time histogram with a log-normal fit of the kap95 translocations can be seen in Figure 5.12 (n=607). The most likely dwell time is **0.15 ms**. The dwell times for an SG coated pore are a lot lower than those of the FG coated pore and comparable with the bare pore.

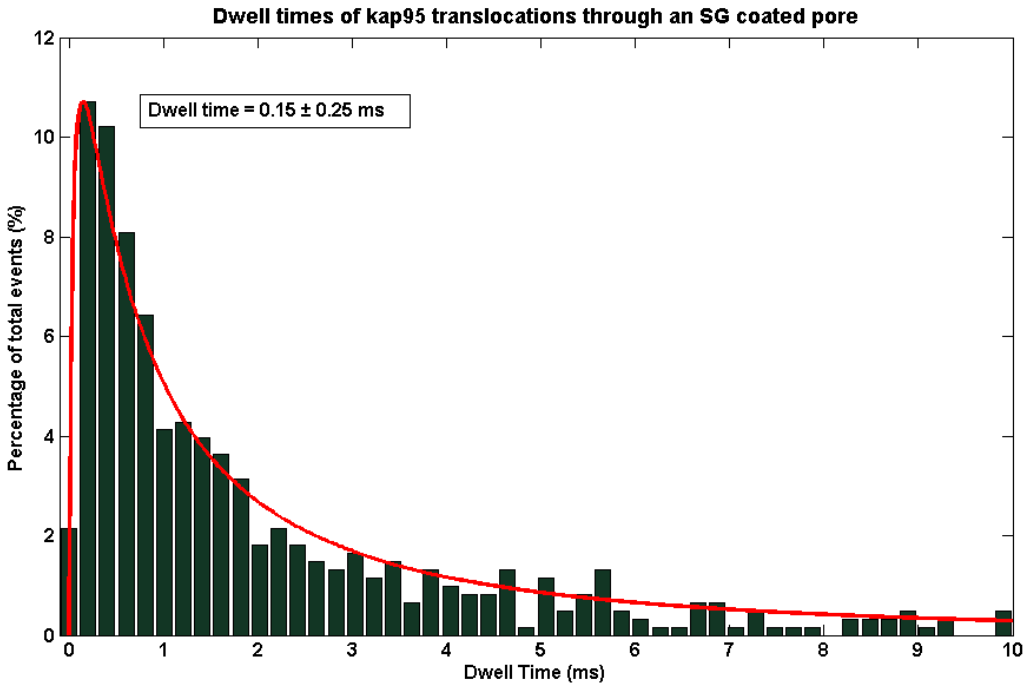

Figure 5.12: Histogram and log-normal fit of dwell times of kap95 translocating through a SG coated pore (n=607). The mode of the log-normal fit is 0.15 ms. The bin width is 0.2 ms.

The conductance blockades caused by the kap95 can be seen in Figure 5.13, with the largest bin at **0.13 nS**. The comparison with Figure 5.2 show a lot of resemblance, only the most likely conductance blockade of kap95 through a SG coated pore is comparable with the translocations through a bare pore.

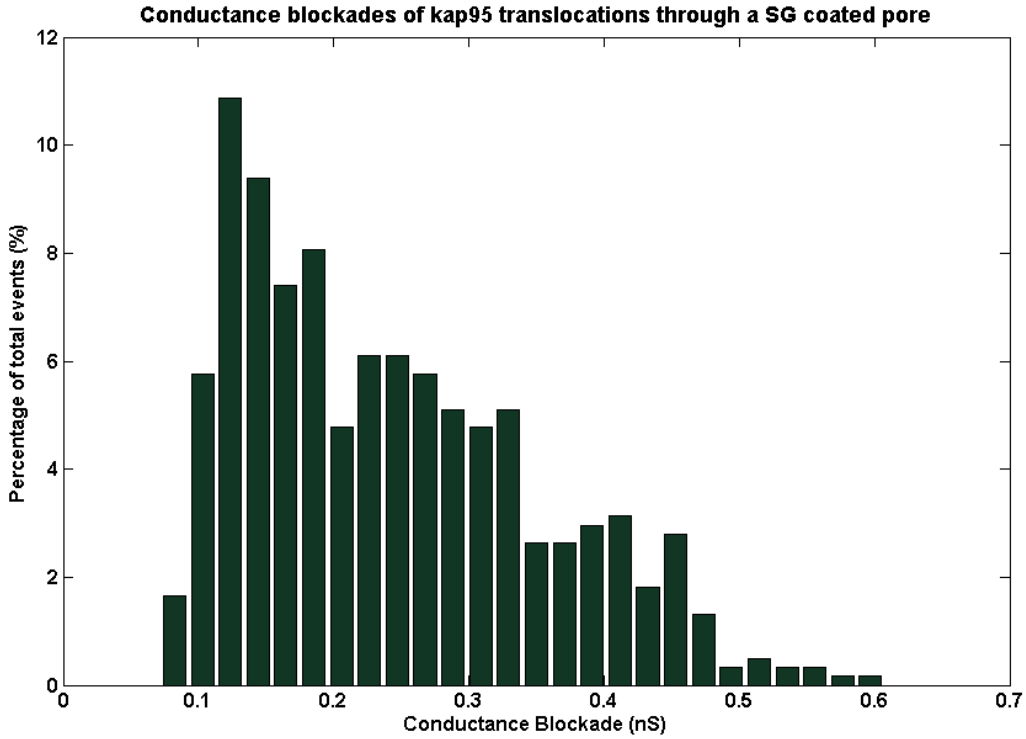

Figure 5.13: Conductance blockades of kap95 translocating through a SG coated pore with n=67. The highest bar is at 0.13 nS. The bin width is 0.02 nS.

5.3.2 tCherry translocations through a SG coated pore

After the failure of tCherry to translocate through the FG coated pore, we now tried translocating the protein through the SG coated pore. Due to a calculation error the concentration of tCherry in this particular experiment was 25 nM instead of the usual 100 nM.

We expected the tCherry to translocate since there is strong evidence that in the absence of FG-repeat regions in the nucleoporins, the (biomimetic) nuclear pore complex loses its discriminatory function. With our biomimetic nanopore we hypothesize that the selective function is lost because the SG nucleoporins fail to form cross links and thus leave a large space in the nanopore unoccupied. This space could give tCherry the ability to translocate through the nanopore. This assumption was correct and we detected tCherry translocations through a SG coated pore. The dwell times of the events can be seen in Figure 5.14 (n=76). The most likely dwell time is **0.48 ms**. The confidence interval on the log-normal fit is quite low due to the low number of events, caused by the aforementioned concentration calculation error. In comparison with the bare pore translocations, tCherry translocates slower through a SG coated nanopore. This could be due to interactions with the nucleoporins.

In Figure 5.15 the conductance blockades of tranlocating tCherry can be seen. The most likely conductance blockade is **0.23 nS**. As was the case for kap95, the conductance blockades of tCherry through a SG coated pore is slightly smaller than through a bare pore.

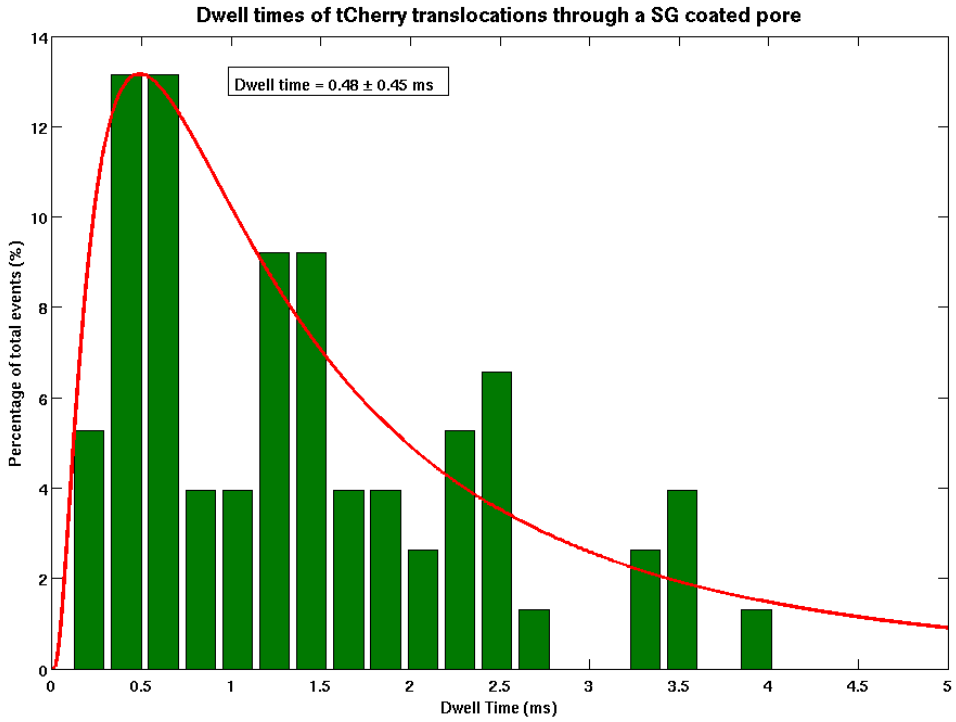

Figure 5.14: Histogram and log-normal fit of the dwell times of tCherry translocating through a SG pore (n=76). The mode of the log-normal fit is 0.48 ms. The bin width is 0.2 ms.

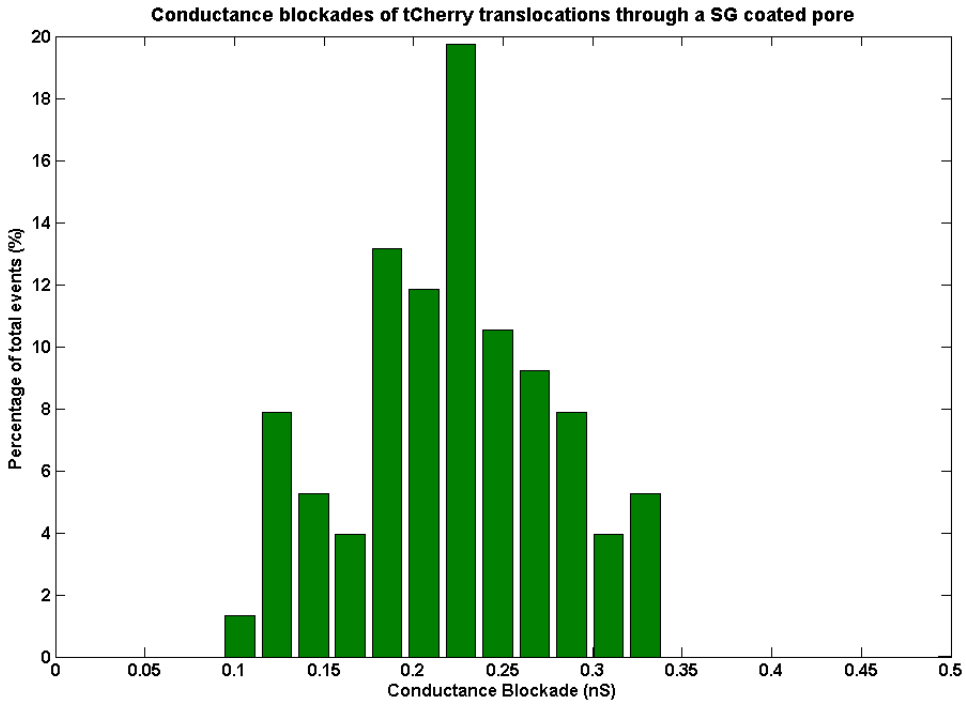

Figure 5.15: Histogram of conductance blockades of tCherry translocating through a SG coated pore (n=76). The most likely conductance blockade is 0.23 nS. The bin width is 0.02 nS.

5.4 Event Frequency of translocations

We started with translocations of kap95 and tCherry (both at 100 nM concentrations) through a bare pore. The event frequencies of the translocations of both proteins can be seen in Figure 5.16. Besides the occasional increase or decrease in event frequency due to random walk behaviour, the frequency stays constant for both proteins , as expected.

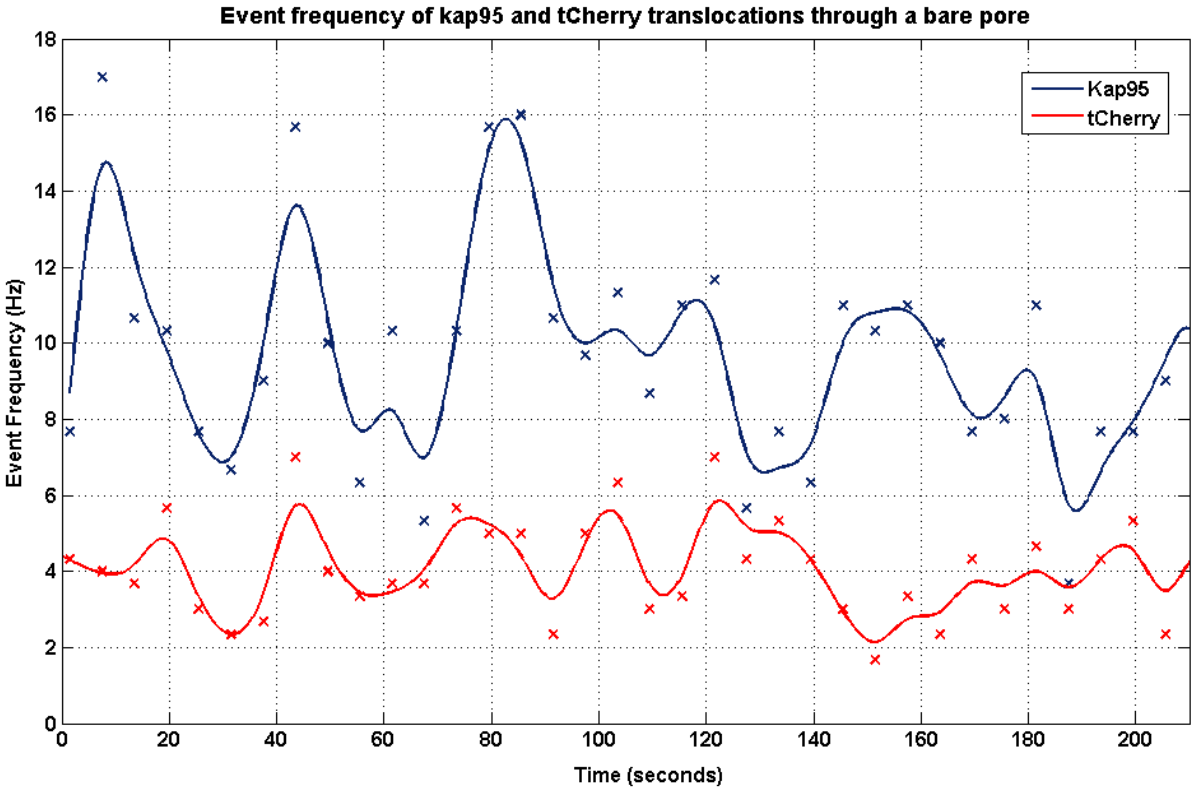

Figure 5.16: Event frequencies of kap95 and tCherry translocations through a bare pore. Kap95 has an average event frequency of 10 Hz and tCherry has an average event frequency of 4 Hz. Crosses indicate data points, the line is smoothed between the data points. Time starts at 0, right after protein was added to the buffer.

When we coated the nanopore with FG nucleoporins the event rate was initially much higher than the bare pore event rate as can be seen in Figure 5.17. After waiting 3 minutes though the event rate dropped to a level that was more in agreement with the bare pore experiments. In Figure 5.17 tCherry through an FG coated pore is not depicted for the simple reason that we did not detect any translocations.

The same behaviour was observed with a SG coated pore and translocating kap95. tCherry translocations through an SG coated pore posed an exception though and the event frequency slowly rised over time. It is important to note however that the concentration of tCherry for the SG-coated translocation experiment, was 25 nM instead of the usual 100 nM, which could explain the low event frequency.

Since the concentration of kap95 on the cis side of the nanopore does not change by a large amount in 3 minutes, there is no reason why the translocation event should change by such a large amount. Therefore, we assume that the high amount of events right after

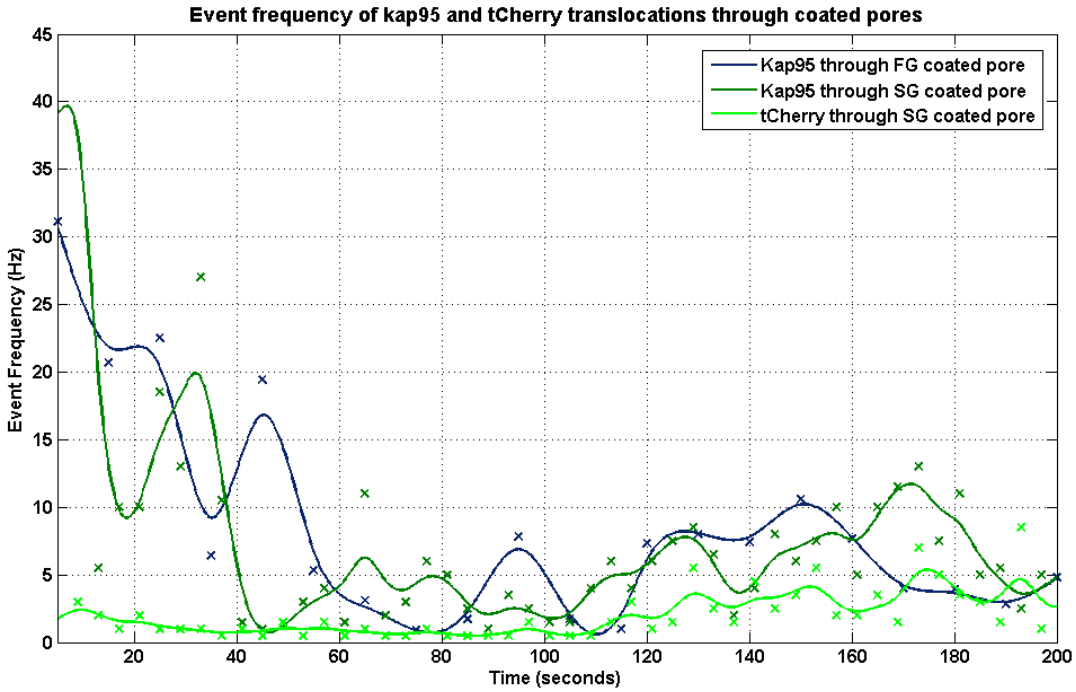

Figure 5.17: Event frequencies of kap95 and tCherry translocations through coated pores. Crosses indicate data points, the line is smoothed between the data points. Time starts at 0, right after proteins are added to the buffer.

adding kap95 into the buffer indicate binding and unbinding events with the FG or SG nups near the pore, instead of translocations. For this reason it is important to wait a few minutes after protein insert before conducting a measurement.

6. Conclusion and Outlook

In this work we set out to answer one of the questions surrounding the nuclear pore complex: Are the FG-repeat regions of nucleoporins responsible for the selective behaviour of an NPC? We started with an introduction of the NPC we were going to mimic. We then introduced the tool we used to carry out the experiments, the solid-state nanopore. We showed that by coating the supporting membrane of the solid-state nanopore with PDMS, we got a superior signal-to-noise ratio, which proved critical for detecting the translocations of our two proteins, kap95 and tCherry. The bare pore translocation of kap95 gave a translocation time of ∼0.17 ms with a most likely conductance blockade of 0.15 nS. The tCherry translocated faster than kap95 through a bare pore, with a dwell time of ∼0.10 ms and a most likely conductance blockade of 0.30 nS. We believe that the shorter dwell time of tCherry can be attributed to its hydrophilicity.

The coating process of a nanopore with nucleoporins was perhaps the biggest hurdle in the entire project. The incubation time with nucleoporins had to be tweaked carefully. Incubation time for a Nsp1 wild-type coated nanopore (FG-coating) was 45 minutes. After the FG-coating we translocated kap95 through the pore. We observed a conductance blockade of the translocations of 0.16 nS, which corresponds with the bare pore translocations, indicating that the translocating molecules are the same. The major difference with the bare pore translocations was the dwell times of the kap95 through the FG-coated pore. About 50% of the detected translocations of kap95 had dwell times higher than 50 ms and the highest observed dwell time was 600 ms. The dwell times were much higher than those for the bare pore, which is most likely due to interactions between the FG-nucleoporins and the translocating kap95. The selectivity of the FG-coated pore has been shown when tCherry failed to translocate through the pore.

The incubation time for the Nsp1 FILV → S was only 20 minutes (SG-coating). The translocation of kap95 through the SG-coated pore was successful and the dwell time was ∼0.15 ms and the conductance blockade was around 0.13 nS. Remarkably the conductance blockades and dwell times were on the same order as that of bare pore translocations, which means that there was no considerable interaction between kap95 and the SG nucleoporins. tCherry was also able to translocate through the SG-coated pore which showed that the mutated version of Nsp1 wild type does not have the discriminatory feature. We assume that the mutated nucleoporins lost their ability to form the compact coating of the nanopores as compared to FG nups. This might be the main reason for losing the selective function. The IV plots shown in Figure 5.5 and Figure 5.10 support the claim. The FG coated pores had an 80% conductance blockade and the SG-coated pore was shown to have 50% of the conductance of a bare pore. This behavior agrees with the previous studies.[33] The dwell time of tCherry through the SG coated pore was ∼0.48 ms and the conductance blockade was around 0.23 nS. In comparison with the bare pore tCherry translocations, the SG coating increases the dwell time slightly and reduces the conductance blockade.

The selectivity of our biomimetic nanopore was lost when we coated the nanopore with Nsp1 FILV → S. We have thus shown that replacing the hydrophobic amino acids

with the hydrophilic amino acid residue serine, the selective function of nucleoporins is lost.

Where can we go from here? With the knowledge that the hydrophobic patches in the nucleoporins are responsible for the selective function in a NPC, we can develop medicine that target the nucleus in a more efficient way. The understanding off the selective mechanism of an NPC could lead to new insights in disease prevention and treatment. But the advantages will not only be applicable to healthcare. By utilizing the selective behaviour of nucleoporins in filters we can purify mixtures of macromolecules with great accuracy, which could in turn lead to new scientific breakthroughs on multiple fronts.

A. Protein information

Kap95

Molecular weight: 94.8 kDa
Theoretical pI value: 4.52

tCherry (tetramer of mCherry)

Molecular weight: $\sim$ 100 kDa
Theoretical pI value: $\sim$ 9

Nsp1 Wild-type

Molecular weight: 65.7 kDa
Amino acid sequence:

```
MSKHHHHSGH HHTGHHHHSG SHHHTGENLY FQGSNFNTPQ QNKTPFSFGT ANNNSNTTNQ   60
NSSTGAGAFG TGQSTFGFNN SAPNNTNNAN SSITPAFGSN NTGNTAFGNS NPTSNVFGSN  120
NSTTNTFGSN SAGTSLFGSS SAQQTKSNGT AGGNTFGSSS LFNNSTNSNT TKPAFGGLNF  180
GGGNNTTPSS TGNANTSNNL FGATANANKP AFSFGATTND DKKTEPDKPA FSFNSSVGNK  240
TDAQAPTTGF SFGSQLGGNK TVNEAAKPSL SFGSGSAGAN PAGASQPEPT TNEPAKPALS  300
FGTATSDNKT TNTTPSFSFG AKSDENKAGA TSKPAFSFGA KPEEKKDDNS SKPAFSFGAK  360
SNEDKQDGTA KPAFSFGAKP AEKNNNETSK PAFSFGAKSD EKKDGDASKP AFSFGAKPDE  420
NKASATSKPA FSFGAKPEEK KDDNSSKPAF SFGAKSNEDK QDGTAKPAFS FGAKPAEKNN  480
NETSKPAFSF GAKSDEKKDG DASKPAFSFG AKSDEKKDSD SSKPAFSFGT KSNEKKDSGS  540
SKPAFSFGAK PDEKKNDEVS KPAFSFGAKA NEKKESDESK SAFSFGSKPT GKEEGDGAKA  600
AISFGAKPEE QKSSDTSKPA FTFGAQKDNE KKTETSC
```

Nsp1 mutated FILV $\rightarrow$ S

Molecular weight: 62.1 kDa
Amino acid sequence:

```
MSKHHHHSGH HHTGHHHHSG SHHHTGENLY FQGSNSNTPQ QNKTPSSSGT ANNNSNTTNQ   60
NSSTGAGASG TGQSTSGSNN SAPNNTNNAN SSSTPASGSN NTGNTASGNS NPTSNSSGSN  120
NSTTNTSGSN SAGTSSSGSS SAQQTKSNGT AGGNTSGSSS SSNNSTNSNT TKPASGGSNS  180
GGGNNTTPSS TGNANTSNNS SGATANANKP ASSSGATTND DKKTEPDKPA SSSNSSSGNK  240
TDAQAPTTGS SSGSQSGGNK TSNEAAKPSS SSGSGSAGAN PAGASQPEPT TNEPAKPASS  300
SGTATSDNKT TNTTPSSSSG AKSDENKAGA TSKPASSSGA KPEEKKDDNS SKPASSSGAK  360
SNEDKQDGTA KPASSSGAKP AEKNNNETSK PASSSGAKSD EKKDGDASKP ASSSGAKPDE  420
NKASATSKPA SSSGAKPEEK KDDNSSKPAS SSGAKSNEDK QDGTAKPASS SGAKPAEKNN  480
NETSKPASSS GAKSDEKKDG DASKPASSSG AKSDEKKDSD SSKPASSSGT KSNEKKDSGS  540
SKPASSSGAK PDEKKNDESS KPASSSGAKA NEKKESDESK SASSSGSKPT GKEEGDGAKA  600
ASSSGAKPEE QKSSDTSKPA STSGAQKDNE KKTESTSC
```

B. Equipment and handling

Equipment

Recording equipment: Axopatch 200B Amplifier

Equipment handling

- The electrodes used for the measurements were created by placing Ag-wire in bleach for 5 minutes and then cleaning with water, ethanol and IPA and then blow dry.

- The flowcells are made of PMMA and were stored in 50% ethanol. Before the measurement they were cleaned with water and ethanol and blow dried with N_2.

- The solid state nanopore is plasma cleaned before a bare pore measurement, by placing it into a plasma chamber for 30 seconds.

7. Acknowledgement

First off all a big thanks to Adithya Ananth for having a lot of patience and providing me with great guidance and awesome ideas. I think it's a great project and like you said, you just have to keep trying, it has to work someday.

I would like to thank Prof. Dr. Cees Dekker for giving me the opportunity to work on such an interesting project.

Thanks to Calin Plesa for writing transalyzer and of course for giving me some great tips and advice. This project would be a dead end if it were not for your suggestion to use PDMS.

I would like to thank our collaborators Steffen Frey and Dirk Görlich at the Max Planck Institute for Biophysical Chemistry, Göttingen, Germany for providing us with the proteins used in these experiments.

Thanks to Stephanie Heerema for letting me use the micromanipulator, and for the useful discussion.

Thanks to Dr. Meng Yue Wu for drilling the nanopores and for providing TEM images of the nanopores.

Also thanks to Magnus Jonsson, Gautam Soni and Daniel Verschueren for the great suggestions and discussions.

Finally, I would like to thank the entire Cees Dekker group and the department of Bionanoscience since they were always there to give some good advice and point the project in the right direction.

8. Bibliography

[1] Wälde, S. & Kehlenbach, R.H. The part and the whole: functions of nucleoporins in nucleocytoplasmic transport. *Trends Cell Biol.*, 20:461–469, 2010.

[2] Frey, S. et al. FG-rich repeats of nuclear pore proteins form a three-dimensional meshwork with hydrogel-like properties. *Science*, 314:815–817, 2006.

[3] Kowalczyk, S.W. et al. Single-molecule transport across an individual biomimetic nuclear pore complex. *Nature Nanotechnology*, 6:433–438, 2011.

[4] Callan, H.G. & Tomlin, S.G. Investigation of the structure of the nuclear membrane by means of the electron microscope. *Proc. R. Soc. Lond. B.*, 137:367–378, 1950.

[5] Reichelt, R. et al. Correlation between structure and mass distribution of the nuclear pore complex and of distinct pore complex components. *J. Cell Biol.*, 110:883–894, 1990.

[6] Tran, E.J. & Wente, S.R. Dynamic nuclear pore complexes: Life on the edge. *Cell*, 125:1041–1053, 2006.

[7] Alber, F. et al. Determining the architecture of macromolecular assemblies. *Nature*, 450:683–694, 2007.

[8] Rout, M.P. et al. The yeast nuclear pore complex: Composition, architecture and transport mechanism. *J. Cell Biol.*, 148:635–651, 2000.

[9] Alber, F. et al. The molecular architecture of the nuclear pore complex. *Nature*, 450:695–700, 2007.

[10] Pante, N. & Kann, M. Nuclear pore complex is able to transport macromolecules with diameters of ∼39 nm. *Mol. Biol. Cell*, 13:425–434, 2002.

[11] Weis, K. The nuclear pore complex: Oily spaghetti or gummy bear? *Cell*, 130:405–407, 2007.

[12] Mohr, D. et al. Characterisation of the passive permeability barrier of nuclear pore complexes. *EMBO J.*, 28:2541–2553, 2009.

[13] Lowe A. et al. Selectivity mechanism of the nuclear pore complex characterized by single cargo tracking. *Nature*, 467:600–603, 2010.

[14] Stewart, M. Structural basis of the nuclear protein import cycle. *Biochem. Soc. Trans.*, 34:701–704, 2006.

[15] Mosammaparast, N. & Pemberton, L.F. Karyopherins: From nuclear-transport mediators to nuclear-function regulators. *Trends in Cell Biol.*, 14:547–556, 2004.

[16] Grünwald, D et al. Nuclear export dynamics of RNA-protein complexes. *Nature*, 475:333–341, 2011.

[17] Ribbeck, K. & Görlich, D. The permeability barrier of nuclear pore complexes appears to operate via hydrophobic exclusion. *EMBO J.*, 21:2509–2841, 2002.

[18] Peters, R. Translocation through the nuclear pore complex: selectivity and speed by reduction-of-dimensionality. *Traffic*, 6:421–427, 2005.

[19] Lim, RY et al. Nanomechanical basis of selective gating by the nuclear pore complex. *Science*, 318:640–643, 2007.

[20] Rout, M.P. et al. Virtual gating and nuclear transport: the hole picture. *Trends in Cell Biol.*, 13:622–628, 2003.

[21] Coulter, W.H. & Hogg, W.R. Apparatus and method for measuring a dividing particle size of a particulate system, January 19 1971. US Patent 3,557,352.

[22] Janssen, X.J.A. et al. Rapid manifacturing of low-noise membranes for nanopore sensors by trans-chip illumination lithography. *Nanotechnology*, 23:475302, 2012.

[23] Edel, J. & Albrecht, T. *Engineered nanopores for bioanalytical applications*. Elsevier, Oxford, UK, 2013.

[24] Hall, J.E. Access resistance of a small circular pore. *The Journ. of Gen. Phys.*, 66:531–532, 1975.

[25] Lide, D.R. (Editor). *CRC Handbook of Chemistry and Physics*. CRC Press, 2004.

[26] Kowalczyk, S.W. et al. Modeling the conductance and DNA blockade of solid-state nanopores. *Nanotechnology*, 22:315101, 2011.

[27] Plesa, C. Transalyzer Software, 2013.

[28] Tabard-Cossa, V. et al. Noise analysis and reduction in solid-state nanopores. *Nanotechnology*, 18:305505, 2007.

[29] Miles, B.N. et al. Single molecule sensing with solid-state nanopores: Novel materials, methods, and applications. *Chem. Soc. Rev.*, 42:15–28, 2013.

[30] Jovanovic-Talisman et al. Artificial nanopores that mimic the transport selectivity of the nuclear pore complex. *Nature*, 457:1023–1027, 2009.

[31] Howarter, J.A. & Youngblood, J.P. Optimization of silica silanization by 3-aminopropyltriethoxysilane. *Langmuir*, 12:1114211147, 2006.

[32] Tomás Magalhães. Solid state nanopores that mimic the selectivity of the nuclear pore complex. Master's thesis, TU Delft, 2010.

[33] Eisele, B. et al. Cohesiveness tunes assembly and morphology of FG nucleoporin domain meshworks Implications for nuclear pore permeability. *Biophy. J.*, 105:1860–1870, 2013.

[34] Plesa, C. et al. Fast translocation of proteins through solid state nanopores. *Nano Lett.*, 13:658–663, 2013.

[35] Yusko, E.C. et al. Controlling protein translocation through nanopores with bio-inspired fluid walls. *Nature Nanotechnology*, 6:253–260, 2011.